HHS Public Access

Author manuscript

Neuroimage. Author manuscript; available in PMC 2015 December 01.

Published in final edited form as:

Neuroimage. 2014 December ; 103: 462–475. doi:10.1016/j.neuroimage.2014.08.029.

Decoupling function and anatomy in atlases of functional connectivity patterns: Language mapping in tumor patients

Georg Langs[a,c,*], **Andrew Sweet**[a], **Danial Lashkari**[a], **Yanmei Tie**[b], **Laura Rigolo**[b], **Alexandra J. Golby**[b], and **Polina Golland**[a]

[a]Computer Science and Artificial Intelligence Lab, Massachusetts Institute of Technology, Cambridge, MA, USA

[b]Department of Neurosurgery, Brigham and Women's Hospital, Harvard Medical School, Boston, MA, USA

[c]Computational Imaging Research Lab, Department of Biomedical Imaging and Image-guided Therapy, Medical University of Vienna, Vienna, Austria

Abstract

In this paper we construct an atlas that summarizes functional connectivity characteristics of a cognitive process from a population of individuals. The atlas encodes functional connectivity structure in a low-dimensional embedding space that is derived from a diffusion process on a graph that represents correlations of fMRI time courses. The functional atlas is decoupled from the anatomical space, and thus can represent functional networks with variable spatial distribution in a population. In practice the atlas is represented by a common prior distribution for the embedded fMRI signals of all subjects. We derive an algorithm for fitting this generative model to the observed data in a population. Our results in a language fMRI study demonstrate that the method identifies coherent and functionally equivalent regions across subjects. The method also successfully maps functional networks from a healthy population used as a training set to individuals whose language networks are affected by tumors.

Introduction

The functional architecture of the cerebral cortex includes regions and networks of regions that become active at different times. The temporal profiles range from brief activity during specific tasks, such as processing of individual visual percepts (Kveraga et al., 2011), to extended periods of resting state in the absence of external stimuli, when the brain is suspected to engage in activities such as memory encoding (Buckner et al., 2008). Functional networks vary spatially across individuals due to natural variability (Saxe et al., 2006; Fedorenko and Kanwisher, 2011), developmental processes in early childhood (Kuhl, 2010) or adulthood (Elbert and Rockstroh, 2004), or due to pathology (Elkana et al., 2009). Reorganization in the cerebral system can occur over remarkably short periods of time

[*]Corresponding author at: Computational Imaging Research Lab, Department of Biomedical Imaging and Image-guided Therapy, Medical University of Vienna, Waehringer Gürtel 18-20, 1090 Vienna, Austria.

(Elbert and Rockstroh, 2004; Scholz et al., 2009). The brain can sustain intact functionality even in the case of substantial damage to anatomical sites due to lesions (Desmurget et al., 2007). In both healthy brains and pathology the relationship between functional connectivity and anatomical organization is complex (Hagmann et al., 2008; Venkataraman et al., 2010). In particular, the relationship between the intrinsic structure of functional networks and the spatial distribution across the cerebral system is currently not well understood.

Our motivation comes from studies of reorganization of language networks caused by a lesion and of the relationship between the resulting network and the degree of recovery from *aphasia* (impairment of language ability). Evidence for a link exists, but the changes in language networks during reorganization are not yet characterized well enough to predict outcomes (Heiss et al., 2003). The spatial patterns of reorganization range from recruitment of neighboring regions to employing areas not typically associated with language (Meyer et al., 2003; Ackermann and Riecker, 2004).While there is considerable variability in outcomes across patients, there is no clear correlation between spatial distribution after reorganization and outcome (Heiss et al., 2003). That is, there is no tight coupling between the function of a cerebral network, and the spatial distribution of its units in the anatomical space.

This raises two immediate questions. First, what aspects of the functional network structure responsible for intact language functionality are independent of the spatial location of the network units? Second, how can we capture those characteristics, and how can we map them across subjects even if substantial differences in the spatial distribution occur? We emphasize that there is a conceptual difference between variability of the spatial distribution of functional units, and variability of function itself. A particularly strong disconnection between the two occurs in the context of displacement or reorganization, when the brain sustains functionality while redistributing functional units across the cortex. How does the actual function change at that point? We cannot tell from observing the spatial activation patterns across a population anymore. We have to study function decoupled from space to observe common networks across subjects despite anatomical differences.

In this paper we do not necessarily answer the questions above, but propose an approach to formulate and test such questions. We develop a novel methodology to capture, compare and summarize the functional structure that emerges during a specific cognitive task in a way that is decoupled from its anatomical location. We build a generative model that summarizes functional characteristics across a population of subjects without relying on consistency of the spatial distribution of activated regions. We argue that this decoupling is necessary for understanding the nature of changes in functional organization, and for differentiating between mere spatial redistribution and fundamental functional reorganization in future experiments. We suggest that the proposed representation can be viewed as an atlas, while at the same time being independent of anatomical and spatial properties of the functional units.

We demonstrate how to learn characteristics of functional networks from a population of individuals, and how to map the learned networks to other subjects. Experimental results indicate that the functional interaction structure active during an experimental condition can serve as a basis to identify functional networks across subjects. This paper extends our preliminary work presented in (Langs et al., 2011). Here we expand the method derivations,

extend the empirical evaluation to include tumor patient data, and introduce a framework to transfer information across subjects via the atlas. We detail the relationship to existing work in the next section.

This paper is organized as follows. In the Background section we discuss atlases and their limitations in the context of brain mapping. In An atlas as a generative model of functional connectivity section we detail the atlas representation as a generative model of functional connectivity, and in the Atlas construction: functional connectivity alignment section we derive the procedure for building the atlas from a population. In the Interpreting new data with help of the atlas section we detail how to use this atlas to interpret new data, in the Evaluation and Results sections we report findings on experimental data. In the Discussion section we discuss these results.

Background

Atlases and population studies

Collecting evidence from multiple individuals, capturing characteristics shared across a population, and summarizing them in a unified representation are central topics of neuroscience. A summary approach ubiquitous in neuroimaging studies results in a population atlas that reflects the common neural organization in a population. The atlas serves two purposes: first, it is a reference coordinate frame or stereotaxic space that serves as a basis for the study and summary of neuroimaging data since it establishes correspondences across multiple subjects. Second, the atlas itself is informative since it captures properties of interest, such as shape variability or activation patterns in the population.

The traditional brain imaging paradigm in most functional MRI (fMRI) studies treats functional activity as a feature of a location within the anatomical coordinate frame. The anatomical variability in a population is mitigated by smoothing and non-rigid registration of the anatomical data into a joint atlas coordinate system. Functional signals are mapped accordingly and the remaining spatial variability of functional regions is typically ignored or treated as a confounding factor. Talairach (Talairach and Tournoux, 1988) and Montreal Neurological Institute (MNI) (Collins et al., 1995) space are two atlas coordinate systems commonly used in practice for mapping and probabilistic detection of regions including widely popular implementations in FSL (Woolrich et al., 2009), Freesurfer (Fischl et al., 2002), and SPM (Friston et al., 1995).

While we can learn a template from healthy subjects via group-wise registration, atlases can also be constructed from subjects affected by pathology. We can learn the statistical properties of shape and tissue across the population, and correlate them with disease progression where large data sets exist such as for the Alzheimer's disease (Mueller et al., 2005). Some existing methods include a temporal component in atlas building, to reflect the dependence of the atlas on time, age, or disease stage (Davis et al., 2010; Dittrich et al., 2014; Wolz et al., 2011). Such an approach depends on anatomic consistency of the pathology and hence is not suitable for lesions such as brain tumors or multiple sclerosis in which the location of the change varies across subjects (Fig. 1).

Limits of spatial atlases

The goal of any atlas is to establish correspondences across examples. Despite being central to modeling populations, the nature of correspondences remains ambiguous, and existing approaches vary significantly on the underlying assumptions they make about the data. Anatomical atlases are based on registering morphology of individuals, and view function as feature of a locationin the reference space once an anatomical match has been achieved. This framework cannot express or account for spatial variability of functional networks within the population since it assumes perfect spatial correspondences when detecting networks by averaging over multiple subjects. This assumption has to be relaxed if the location of a functional unit is known to vary across subjects. For example, many studies of high-level function first identify functional regions of interest (fROIs) in individuals to cope with common spatial variability, and only then study the responses in the resulting small number of fROIs (Saxe et al., 2006; Fedorenko et al., 2010). This approach is based on detection results for each subject, which can be infeasible if the activation is weak and cannot be distinguished from noise in individual subjects without averaging over the group. Intermediate approaches integrate functional information in the alignment of cortical surfaces (Sabuncu et al., 2010a), or adapt the registration cost function to the specific task of functional alignment (Yeo et al., 2010). Correspondence across a population might even be impossible to establish if substantial differences exist and multiple templates are necessary to represent its variability (Sabuncu et al., 2010b), or if pathology has altered morphology. A recently proposed approach of Haxby et al. (2011) represents response patterns to different stimuli observed in fMRI data of the ventral temporal cortex in a high-dimensional space that enables decoding across subjects. The global interaction structure that emerges during cognitive processes is typically not considered by the methods demonstrated to date.

Decoupling function and space

In this paper we demonstrate that the interaction patterns can serve as the basis to identify functional networks across subjects independently of their spatial distribution. We do not assume a tight coupling between anatomical location and function, but view functional signals as the basis of a descriptive map that represents a global connectivity pattern associated with a particular specific cognitive process. We develop a representation of those networks based on manifold learning techniques and demonstrate an algorithm for learning an atlas from a population of subjects performing the same task. Our main assumption is that the connectivity pattern associated with a functional process is a fundamental characteristic, and is consistent across individuals. Accordingly, we construct a generative model (atlas) for these connectivity patterns that describes the common structures across individuals in a population.

The immediate clinical goal of our work is to provide additional evidence for localization of functional areas. A robust localization approach is important for neurosurgical planning if individual activations are weak or if displacement or reorganization is due to pathologies such as tumor growth. Furthermore the method provides a basis for understanding the mechanisms underlying formation and reorganization in the cerebral system.

Related work

A spectral embedding (Von Luxburg, 2007) represents data points in a map that reflects a large set of pairwise affinity values in the Euclidean space. Diffusion maps establish a metric based on the concept of diffusion processes on a graph (Coifman and Lafon, 2006). A probabilistic interpretation of diffusion maps has also been proposed (Nadler et al., 2007). A probabilistic generative model that establishes a link between the embedding coordinates and a similarity matrix has been demonstrated in (Rosales and Frey, 2003). Previously demonstrated spectral methods in application to fMRI analysis mapped voxels into a space that captured joint functional characteristics of brain regions in individual subjects (Langs et al., 2008). This approach represents the magnitude of co-activation by the density in the embedding. Functionally homogeneous units have been shown to form clusters in the embedding in a study of parceled resting-state fMRI data (Thirion et al., 2006). Thirion and Faugeras (2004) used non-linear embedding for fMRI analysis in individual subjects, group-level analysis relying on spatial correspondence across subjects was investigated by Craddock et al. (2012). In Friston et al. (1996) multidimensional scaling was employed to retrieve a low dimensional representation of positron emission tomography (PET) signals in a set of activated regions. In an approach closely related to the method proposed in this paper (Langs et al., 2010), an embedding of fMRI signals was used to match corresponding functional regions across different subjects.

An atlas as a generative model of functional connectivity

We use a probabilistic formulation of diffusion maps to embed fMRI signals, and to summarize the resulting patterns across the atlas population. We start by reviewing the original diffusion map formulation. We then derive a probabilistic likelihood model for the data based on this mapping and use the model to link diffusion maps of functional connectivity across subjects. The core concept is illustrated in Fig. 2. We seek to learn an atlas in the embedding space. Every voxel in each subject is mapped to a point in the embedding space. The atlas represents all voxels in the individual fMRI data. Point positions in the embedding space respect their mutual functional connectivity shared across the entire population.

From fMRI time courses to connectivity matrices and embedding coordinates

Given an fMRI sequence $\mathbf{I} \in \mathbb{R}^{T \times N}$ that contains N voxels, each characterized by an fMRI signal over T time points, we calculate a pairwise similarity matrix $\mathbf{W} \in \mathbb{R}^{+N \times N}$ that assigns a non-negative symmetric weight to each pair of voxels (i, j):

$$\mathbf{W}(i,j) = e^{\frac{\langle \mathbf{I}_i, \mathbf{I}_j \rangle}{\varepsilon}}, \quad (1)$$

where $\langle \cdot, \cdot \rangle$ is the correlation coefficient of the time courses $\mathbf{I}_i$ and $\mathbf{I}_j$, and ε controls the weight decay. We define a graph whose vertices correspond to voxels and whose edge weights are determined by $\mathbf{W}$ (Coifman and Lafon, 2006; Langs et al., 2008). In practice, we discard all edges that have a weight below a chosen threshold. This construction yields a graph with low edge density which is then transformed into a Markov chain. We define the Markov transition matrix $\mathbf{P} = \mathbf{D}^{-1}\,\mathbf{W}$, where $\mathbf{D}$ is a diagonal normalization matrix such that

$d_i = \mathbf{D}(i, i) = \sum_j w(i, j)$ is the strength of node i. By interpreting the entries $\mathbf{P}(i, j)$ as transition probabilities of a random walk (Meila and Shi, 2001), we can define the diffusion distance parameterized by the diffusion time t:

$$D_t(i,j) = \sum_{i'=1,\ldots,N} \frac{\left(\mathbf{P}^t(i,i') - \mathbf{P}^t(j,i')\right)^2}{\phi(i')} \text{where} \phi(i) = \frac{d_i}{\sum_{i'} d_{i'}}. \quad (2)$$

The transition probabilities are based on the functional connectivity of node pairs; the diffusion distance integrates the connectivity values over possible paths that connect two points and defines a geometry that captures the entirety of the connectivity pattern. This distance is characterized by the operator $\mathbf{P}^t$, the tth power of the transition matrix. The value of the distance $D_t(i, j)$ is low if there is a large number of paths of at most length t steps with high transition probabilities between the nodes i and j. Defining the distance by all possible paths up to a certain length, as opposed to the geodesic distance, results in relative robustness to noise (Coifman and Lafon, 2006). Setting maximal path length, or diffusion time, restricts the size of the neighborhood in the connectivity graph that influences distance values. This parameterization provides control of the granularity of the embedding, and at the same time preserves stability, even if the entire graph becomes very large (Von Luxburg et al., 2010).

The diffusion map coordinates $\mathbf{\Gamma} = [\gamma_1, \gamma_2, \cdots, \gamma_N]^T$ yield a low-dimensional embedding of the signal such that the resulting pairwise distances approximate diffusion distances, i.e., $\|\gamma_i - \gamma_j\|^2 \approx D_t(i, j)$ (Nadler et al., 2007). They are derived from the right eigenvectors of the transition matrix. In Appendix A we show that a diffusion map can be viewed as a solution to a least-squares problem. We construct a symmetric matrix $\mathbf{A} = \mathbf{D}^{-1/2}\mathbf{W}\mathbf{D}^{-1/2}$ that is adjoint to $\mathbf{P}$ (Nadler et al., 2007), and define

$$\mathbf{L} = \mathbf{D}^{-1/2}\mathbf{A}^{2t}\mathbf{D}^{-1/2}. \quad (3)$$

We treat matrix $\mathbf{L}$ as the observation, and obtain $L_1, \ldots, \mathbf{L}_S$ for S subjects as illustrated in Fig. 2. The embedding coordinates are then found as follows:

$$\mathbf{\Gamma}^* = \underset{\Gamma \in \mathbb{R}^{N \times L}}{argmin} \sum_{i,j} d_i d_j \left(\mathbf{L}(i,j) - \gamma_i^T \gamma_j\right)^2, \quad (4)$$

where L is the dimensionality of the embedding. To simplify notation, we omit t for $\mathbf{L}$ and $\mathbf{\Gamma}$ in the derivations, assuming that all the results are derived for a fixed, known diffusion time.

As an aside, many embedding methods work with the normalized graph Laplacian $Lap^{norm} = \mathbf{I} - \mathbf{D}^{-1}\mathbf{W} = \mathbf{I} - \mathbf{P}$. It can be shown that the largest eigenvalues of the transition matrix $\mathbf{P}$ correspond to the smallest eigenvalues of Lap^{norm} and for each eigenvector with eigenvalue λ_P of $\mathbf{P}$ there is an identical eigenvector with eigenvalue $\lambda_{Lap} = 1 - a_P$ of Lap^{norm} (Von Luxburg, 2007).

The weight threshold in the graph construction is typically chosen so that the graph remains connected (Coifman and Lafon, 2006). One can also interpret it as the liberal value below

which weights are likely to be generated by noise (He et al., 2009). The weight decay parameter ε controls the step size, or the first order neighborhood for a random walk on the graph (Nadler et al., 2007). The diffusion time t then extends random walks to larger neighborhoods by parameterizing the family of diffusion distances corresponding to the powers of the transition matrix $\mathbf{P}^t$, and acts as a scaling parameter (Lafon and Lee, 2006). Hence while ε controls the connectivity on the most local scale, increasing t allows for integrating evidence from multiple connections between two points to determine their closeness. The spectrum of $\mathbf{P}^t$ informs us about the graph structure, and is between the two extremes of a fully connected graph (only one non-zero eigenvalue) and a set of unconnected points (all eigenvalues equal 1). The distance can be estimated with accuracy δ by the Euclidean distance in the embedding, if the L largest eigenvectors are used, $|\lambda_L|^t > |\delta\lambda_1|^t$, and λ_1 is the largest non-trivial eigenvalue. Thus, given an accuracy constraint δ we need fewer eigenvectors if the spectrum falls off more rapidly, which corresponds to an overall stronger connectivity in the graph.

A generative model for diffusion maps across subjects

To construct an atlas in the embedding space from a population we view the relationship between the embedding coordinates and the affinity matrix as a generative process. The goal of the generative model is to jointly explain the distribution of pairwise functional affinities of voxels across all subjects. Latent variables $\mathbf{\Gamma} = \{\mathbf{\Gamma}_s\}_{s=1}^{S}$ correspond to the diffusion map coordinates representing the fMRI voxels for S subjects indexed by $s \in \{1,\ldots, S\}$ (Fig. 2). The matrix $\mathbf{L}_s$ of subjects is treated as a noisy observation of $\mathbf{\Gamma}_s$. A joint mixture distribution in the embedding space serves as a prior for the points in each distribution $\mathbf{\Gamma}_s$, $1 \le s \le S$.

We can interpret Eq. (4) as maximization of a Gaussian likelihood model. We let γ_{si} denote the embedding coordinates of voxel i in subject s and let $\mathbf{L}_s$ be the observation matrix for subject s.We further assume that elements of $\mathbf{L}_s$ are conditionally independent given the embedding coordinates:

$$\mathbf{L}_s(i,j) = \gamma_{si}^T \gamma_{sj} + \varepsilon_{sij}, \text{where} \varepsilon_{sij} \sim \mathcal{N}\left(0, \frac{\sigma_s^2}{d_{si} d_{sj}}\right). \quad (5)$$

Here, $\mathcal{N}(\cdot;\mu,\sigma^2)$ is a Gaussian distribution with mean μ and variance σ^2.We note that the variance depends on the node strength values d_i, d_j, which is technically a problem since these quantities depend on the data $\mathbf{W}$. We find that in practice, the method works well and leave the development of rigorous probability models for diffusion maps as an interesting future direction.

In the absence of a prior distribution on $\mathbf{\Gamma}_s$, fitting this model to the data yields results similar to the conventional diffusion maps for each subject constructed independently from the rest of the population. Our goal is to define an atlas that represents a population-wide structure of functional connectivity in the space of diffusion maps. To capture this common structure, we define a shared prior distribution on the embedding coordinates $\mathbf{\Gamma}_s$ for all subjects, and expect the embedded vectors to be in correspondence across subjects. Here, we assume that the common distribution in the embedding space is a mixture of K Gaussian

components. We let $z_{si} \in \{1, \cdots, K\}$ be the component assignment for voxel i in subject s and construct the prior on the embedding coordinates of voxel i in subject s:

$$p(\gamma_{si}|z_{si}=k;\boldsymbol{\mu},\Theta)=\mathcal{N}(\gamma_{si};\mu_k,\Theta_k), \quad (6)$$

where μ_k and Θ_k are the mean and covariance matrix for component k. We let the component assignments be independently distributed according to the weights of different components, i.e.,

$$p(z_{si}=k)=\pi_k. \quad (7)$$

Together, Eqs. (5)– (7) define the joint distribution of the fMRI voxel representatives in the embedding space $\boldsymbol{\Gamma}=\{\boldsymbol{\Gamma}_s\}_{s=1}^{S}$, the component assignments $\{z_{si}\}$, and the observed affinities $\boldsymbol{L}=\{\mathbf{L}_s\}_{s=1}^{S}$. The distribution is parameterized by component centers $\{\mu_k\}$, covariance matrices $\{\Theta_k\}$, weights $\{\pi_k\}$, and data noise σ_s^2.

By adding the group prior over diffusion maps, we constrain the resulting subject maps to be aligned across subjects and further encourage them to resemble the population-level structures characterized by the mixture model. The mixture model in Eqs. (6) and (7) acts as a population atlas in the embedding space. While the data term is specific for each individual subject, the mixture model is shared across the entire population. Fig. 2 illustrates this relationship, which is also central during the learning of the atlas.

Atlas construction: functional connectivity alignment

We learn the atlas from observed population data represented by the matrix $\mathbf{L}_s$ of all subjects with a variational expectation maximization (EM) algorithm (Jaakkola, 2000). During optimization we estimate the coordinates of the mapped representations of all voxels in all fMRI data in the joint embedding space $\boldsymbol{\Gamma}$ together with the parameters of the GMM $\{\mu_k, \Theta_k, \pi_k\}$ that define the prior distribution. Using the variational approach, we approximate the posterior distribution $p(z, \boldsymbol{\Gamma}|\boldsymbol{L})$ of the latent variables with a product distribution

$$q(\boldsymbol{\Gamma}, z)=\prod_{s,i} q(\gamma_{s,i})\, q(z_{s,i}). \quad (8)$$

The problem reduces to minimization of the Gibbs free energy

$$\mathcal{F}=-\mathbb{H}(q)-\mathbb{E}_q[\log p(\boldsymbol{\Gamma}, z, \mathrm{L};\mu, \Upsilon, \pi)], \quad (9)$$

where $\mathbb{H}(q)$ is the entropy of the distribution $q(\cdot)$ and $\mathbb{E}_q$ is the expected value operator for the same distribution. We derive coordinate descent update rules that, given an initialization of all latent variables and parameters, find a local minimum of the cost function in Eq. (9). The detailed derivation of the update rules is presented in Appendix B. Once the algorithm converges, it produces the estimates of the model parameters $\{\mu_k, \Theta_k, \pi_k\}_{k=1}^{K}$ and the coordinates representing all embedded voxels of all subjects in the joint embedding space $\{\boldsymbol{\Gamma}_s\}$.

Initialization

To initialize the algorithm, we first perform embedding separately for each subject. We then randomly choose one subject r to serve as reference and align embedding coordinates $\mathbf{\Gamma}_s$ of each subject to the embedding coordinates $\mathbf{\Gamma}_r$ of the reference subject.

In general, the relationship between the diffusion map coordinates $\mathbf{\Gamma}$ and the corresponding symmetric matrix $\mathbf{L}$ is defined up to an arbitrary orthonormal matrix $\mathbf{Q}$ since $(\mathbf{\Gamma Q})(\mathbf{\Gamma Q})^{\mathrm{T}} = \mathbf{\Gamma Q Q}^{\mathrm{T}}\mathbf{\Gamma}^{\mathrm{T}} = \mathbf{\Gamma\Gamma}^{\mathrm{T}} = \mathbf{L}$. $\mathbf{Q}$ is a transformation that can rotate, flip coefficient signs, and reorder coefficient dimensions, or an *isometry* that leaves distances among points in the embedding space unchanged. In order to define an atlas of the functional connectivity across all subjects, we seek matrix $\mathbf{Q}_s$ for each subject s such that the maps $\{\mathbf{\Gamma}_s\mathbf{Q}_s\}_{s=1}^{S}$ are aligned in a common coordinate frame. Consider aligning the diffusion map $\mathbf{\Gamma}_s$ of subject s to the diffusion map $\mathbf{\Gamma}_r$ of reference subject r.We can performinter-subject registration in two ways: (1) Inter subject signal correlation: Similar to the construction of the diffusion map, we compute the inter-subject affinities between the fMRI signals of subjects s and r using Eq. (1) and only keep those with a correlation above a pre-specified threshold. This step produces a set of M node pairs $\{(i_m, j_m)\}_{m=1}^{M}$, characterized by affinities $\{w_m\}_{m=1}^{M}$. (2) Distance after registration to a common anatomical template: Alternatively the node pairs $\{(i_m, j_m)\}_{m=1}^{M}$ can be matched and characterized by their distance after the anatomical data of both subjects has been mapped to a common template space (e.g., MNI). In the latter case no inter-subject signal correlation enters the registration process explicitly at any point. Then, initialization should ensure that nodes with similar fMRI signals are close in the common embedding space. Therefore, we choose matrix $\mathbf{Q}$ that minimizes the weighted Euclidean distance between pairs of corresponding embedding coordinates

$$\mathbf{Q}^*_{sr} = \underset{\mathbf{Q}}{\operatorname{argmin}} \left[\sum_{m=1}^{M} w_m \| \mathbf{Q}\gamma_{si_m} - \gamma_{rj_m} \|^2_{L_2} \right]. \quad (10)$$

Let $\mathbf{\Gamma}_{s_m} = [\gamma_{si_1}, \ldots, \gamma_{si_M}]^{\mathrm{T}}$ and $\mathbf{\Gamma}_{r_m} = [\gamma_{rj_1}, \ldots, \gamma_{rj_M}]^{\mathrm{T}}$ be matrices holding the embedding coordinates of a random set of matched points for subject s and the reference subject r, respectively. Then, it can be shown that $\mathbf{Q}_{sr}{}^{*} = \mathbf{VU}^{\mathrm{T}}$, where $\mathbf{U}$ and $\mathbf{V}$ are constructed via the singular value decomposition $\mathbf{U\Sigma V}^{T} = \mathbf{\Gamma}^{\mathrm{T}}_{s_m} \operatorname{diag}(\mathbf{W}_m) \mathbf{\Gamma}_{r_m}$ (Scott and Longuet-Higgins, 1991).

We fit a K component Gaussian mixture model (GMM) to the initial estimates of the atlas embedding coordinates $\{\mathbf{\Gamma}_s\mathbf{Q}^*_{sr}\}_{s=1}^{S}$ of a randomly chosen reference subject r to obtain initial estimates of model parameters $\{\mu_k, \Theta_k, \pi_k\}_{k=1}^{K}$. Then we optimize the GMM parameters, and the embedded representations $\mathbf{\Gamma} = \{\mathbf{\Gamma}_s\}_{s=1}^{S}$ of all fMRI voxels in the joint embedding space by minimizing the cost function in Eq. (9) as described above.

Interpreting new data with help of the atlas

Once constructed, the atlas can be used to interpret new data. By interpretation, we mean the transfer of information learned from the atlas population to a new target case, or more

generally transfer of information across multiple subjects, using the correspondences established by learning the atlas. This procedure is analogous to using an anatomical atlas template to transfer, for example, annotations of brain areas to a new subject.

Alignment of one map to the atlas

To transfer information from the atlas to a new subject, we align the target subject to the atlas in the shared embedding space. That is, for a new subject *u* we first calculate the diffusion map coordinates $\mathbf{\Gamma}_u$ and then find a transformation that aligns $\mathbf{\Gamma}_u$ to the atlas distribution $\mathbf{\Gamma}_A$. In our experiments we used the orthonormal alignment described in the Atlas construction: functional connectivity alignment section to find a matrix $\mathbf{Q}_u^*$ that minimizes Eq. (10) with randomly chosen points $\mathbf{\Gamma}_u^M = [\gamma_{u,1}, \cdots, \gamma_{uM}]^{\mathrm{T}}$ matched to $\mathbf{\Gamma}_A^M = [\gamma_{A1}, \cdots, \gamma_{AM}]^{\mathrm{T}}$. The alignment results in positions $\mathbf{\Gamma}_u^A = \mathbf{\Gamma}_u \mathbf{Q}_u^*$ that assign each voxel in the target subject a position in the joint embedding space of the atlas.

Transferring labels from the atlas to an individual case

After registering the target subject to the atlas we transfer labels that delineate the region of activity from the atlas to the subject as illustrated in Fig. 3. For each location in the atlas space, we assign a label based on the samples at positions $\mathbf{\Gamma}_A$. Each voxel i_u (i = 1, 2, …, N_u) in the target subject corresponds to an aligned embedding coordinate γ_{ui} in the joint atlas space. To illustrate the transfer, in our experiments we estimate labels $L_u(i)$ for voxels in the target subject given values for all voxels observed in the atlas population $L_A = \left[L_A^1, \ldots, L_A^{N_A}\right] = [L_1(1), \ldots, L_1(N_1), \ldots, L_s(N_s)]$ and corresponding joint embedding coordinates $\mathbf{\Gamma}_A$, by assigning the value of the nearest neighbor to the target voxel, i.e., $L_u(i) = L_A^{\hat{k}}$ where $\hat{k} = argmin(\|\gamma_A^k - \gamma_{ui}\|)$.

Evaluation

The focus of our evaluation procedure is (1) to investigate the stability of the atlas and its power to represent and map subject-specific characteristics across the atlas population in a joint map; (2) to evaluate if the atlas can serve as a predictor for activity, i.e., if we can sample from the continuous distribution of the atlas, and transfer features to new data after alignment to the atlas; and (3) to assess the differences between mapping within a control population and mapping to tumor patients for whom reorganization is suspected to have taken place.

Stability and specificity

We hypothesize that working in the embedding space should allow us to capture the functional structure common to all subjects more robustly than using fMRI activation signals alone. In order to validate this assumption, we compare the consistency of clustering patterns found in the space of fMRI time courses (*Signal*), a low-dimensional (L = 20) PCA embedding of these time courses (*PCA-Signal*), and the low-dimensional (L = 20) embedding proposed in this paper. We also compare results for the initial alignment (*Linear-Atlas*) and the result of the algorithm after convergence (*Atlas*).

For all approaches (*Signal*, *PCA Signal*, *Linear Atlas*, and *Atlas*) we first apply clustering in each individual subject separately to find subject-specific cluster assignments. We then apply clustering to data combined from all subjects to construct the corresponding group-wise cluster assignments. This latter clustering captures the feature distribution in the joint representation across the entire population. By comparing to subject-specific clustering, we evaluate how well the joint representation captures the functional characteristics observed in individuals. Since our group atlas for the lower-dimensional space is based on a mixture model, we also choose a mixture model for clustering in the *Signal* and *PCA-Signal* spaces. In both cases, each component in the mixture is an isotropic von Mises–Fisher distribution, defined on a hyper-sphere after centering and normalization of the fMRI signals to unit variance (Lashkari et al., 2010).

Likewise, we cluster the diffusion map coordinates $\mathbf{\Gamma}_s$ separately in each subject to obtain subject-specific assignments. We cluster the diffusion map coordinates of all subjects aligned to the first subject $\{\mathbf{\Gamma}_s\mathbf{Q}_{s,1}\}$ for the *Linear-Atlas* and then cluster the final embedding coordinates $\{\mathbf{\Gamma}_s\}$ for the full alignment atlas to obtain group-wise clustering assignments. Analyzing the consistency of clustering labels across methods evaluates how well the population model captures the individual embeddings. For the diffusion maps, Euclidean distance is a meaningful metric; we therefore use a mixture model with Gaussian components that share the same isotropic variance (equivalent to a k-means clustering) for the linear atlas and the initialization of the variational expectation maximization.

To handle the arbitrary cluster labeling, we match group-level clusters and subject-specific clusters by solving a bipartite graph matching problem. We find a one-to-one label correspondence that maximizes voxel overlap between pairs of clusters, similar to the method used in (Lashkari et al., 2010). After matching the cluster labels, we use the voxel set overlap (Dice, 1945) between voxels assigned to a certain cluster by group-level clustering, and those voxels assigned to the corresponding cluster by subject-specific clustering. This step evaluates the consistency between group-level and subject-specific assignments for each cluster. High overlap indicates that the group-level assignment agrees with the subject-specific assignment, while at the same time matching subject-specific patterns across the entire population. We also performed comparison with dual regression ICA (Erhardt et al., 2011) on the same data. We used GroupICAT v3.0a[1] for Matlab, ICASSO with 5 ICA runs, standard PCA, 3 reduction steps, and 20, 15 and 7–12 components.

Transferring features in the atlas space

We also evaluate whether activations can be accurately transferred from the atlas population to an individual subject via the model. We use the response to the experimental paradigm to investigate if the atlas reflects meaningful structure in the functional data. Successful prediction of activation in a single subject from an atlas indicates that the atlas matches specific functionally equivalent areas across a population and enables transfer to independent data. We perform three experiments: (1) transfer within the atlas population, (2)

[1] http://mialab.mrn.org/software/gift/.

transfer from the atlas population to a hold-out subject in a leave-one-out cross-validation and (3) transfer from a healthy atlas population to tumor patients.

After constructing the atlas we evaluate how well the activations from all but one atlas subject predict the activation of the remaining subject. Examining the prediction informs us about the consistency of the atlas alignment, and assesses the utility of the underlying alignment for group studies. For each position in the atlas space we obtain an activation value via the commonly used fixed effects (FFX) GLM activation detection (Friston et al., 1995) in all control subjects. For each point in the fMRI data of the target subject, the activation value is predicted by the value at the corresponding atlas position in the functional space as described in the Interpreting new data with help of the atlas section. To test if the predicted activation matches the subject activation, we also perform subject-level GLM analysis in the target subject.

We perform two evaluations for the control cohort: (1) to test if the atlas establishes valid functional correspondences we predict activations within the atlas cohort; (2) to test if the atlas can serve as predictor for new subjects that are not part of the atlas cohort, we perform leave-one-out cross validation on the set of control subjects.

Analogously, we evaluate the prediction of activation in patients who are not part of the atlas. We build an atlas from the fMRI data of six control subjects who performed the language task. We map active regions to tumor patients who performed the same language task. We then compare the overlap between the predictions and the actual GLM activations in the patients for a range of activation thresholds.

In both cases, we compare functional alignment with non-linear registration (NFIRT) to an MNI template using FSL (Woolrich et al., 2009) that uses a high quality anatomical T1 MRI scan for alignment. The set of grey matter voxels for the evaluation of both anatomical and functional alignment is identical, and is identified by FSL.

Results

We illustrate the method on functional neuroimaging data acquired while subjects were performing a language processing task.

Data

We demonstrate the method on language task fMRI data in six healthy control subjects and seven patients with tumors. The fMRI data was acquired using a 3T GE Signa system (General Electric, Milwaukee, WI, USA), with single-shot gradient-echo echo-planar imaging (EPI) (TR = 2 s, TE = 40 ms, ip angle = 90°, FOV = 25.6 cm, acquisition matrix = 80 × 80, reconstruction matrix=128 × 128, 27 axial slices, ascending interleaved sequence, slice gap=0 mm, voxel size of 2 ×2 × 4mm^3)with a quadrature head coil. Pre-processing of functional data included rigid body motion correction by realigning the images to the first image of the functional run, and high-pass filtering (> 0.0078 Hz) to remove slow drifts. Whole brain T1-weighted axial 3D-SPGR (spoiled gradient recalled) structural images (TR=7.5 s, TE=30ms, ip angle=20°, acquisition matrix = 256 × 256, reconstruction matrix =

512 × 512, voxel size = 0.5 × 0.5 × 1 mm^3, 176 slices) were acquired using array spatial sensitivity encoding technique (ASSET, i.e., parallel imaging) and an 8-channel head coil to obtain corresponding anatomical data. The anatomical data was registered to the functional data. Computation was restricted to grey matter segmented using FSL (Woolrich et al., 2009) on the T1 data. The grey matter labels were transferred to the co-registered fMRI volumes. The language task (antonym generation) block design was identical for all subjects and patients (Suarez et al., 2008; Tie et al., 2009). It was 5 min 10 s long, starting with a 10 s pre-stimulus period. Eight task blocks and seven rest blocks, 20 s each, alternated in the design. The stimuli consisted of words that are part of antonym pairs (e.g., left–right, off–on, push–pull, north–south), subjects had to verbalize the antonym to a word stimuli with minimal movement of head, jaw, and lips. For each subject, an anatomical T1 MRI scan was acquired and registered to the functional data. Grey matter was segmented using FSL (Woolrich et al., 2009) on the T1 data. The grey matter labels were transferred to the co-registered fMRI volumes, and computation was restricted to all voxels in the grey matter. We included seven patients (right handed, 4 females/3 males) with a variety of lesions in the study, for whom presurgical language mapping was performed, and for whom the location of the lesion was sufficiently close to language areas that the risk of displacement existed. The lesions included one ganglioglioma, two metastatic adenocarcinoma, two glioblastomas, one anaplastic oligoastrocytoma, and one oligoastrocytoma. Five lesions were located in the left temporal area, one was located in the left frontal area, and one ranged in the left parietal, and left temporal area. During pre-operative testing, three patients had speech difficulty, four patients exhibited normal language function. A table with the information regarding diagnosis, tumor size and location and language function is given in Appendix C in Table 1.

Implementation details

We construct an atlas from all healthy subjects. For the results presented in this paper, we set the dimensionality of the diffusion map to be $L = 20$ and choose a diffusion time $t = 2$ that satisfies $(\lambda_L/\lambda_1)^t < 0.2$ for all subjects (see From fMRI time courses to connectivity matrices and embedding coordinates section for discussion of parameters). To accelerate computation we only keep grey matter voxels whose degree in the sparsified connectivity matrix is above a certain threshold. In the experiments reported here we choose a threshold of 100. In the EM algorithm, we set the standard deviation of the likelihood model to $\sigma_s = 10^2 N_s^{-1} \sum_i d_{si}$ for the first 10 iterations, then allow this parameter to update for the remaining iterations according to the rule defined in Appendix B. In our experiments, the initial value of σ_s leads to the lowest Gibbs free energy. Activation detection was performed via a generalized linear model (GLM); group-level inference in the atlas population employed commonly used fixed effect analysis (FFX).

Atlas stability

Fig. 4 reports the consistency of clusters between group-level and subject-specific assignments, measured in terms of volume overlap (Dice score) averaged across subjects. In addition, the color of the bars indicates the correlation of the average fMRI signal in each cluster with the fMRI language paradigm convolved with the hemodynamic response function (HRF). We emphasize that the paradigm was not used at any point during the

generation of the maps, the alignment, or the clusters. For a large range of cluster numbers, the cluster whose average signal has the highest correlation with the paradigm is also most stable across subjects. That is, clustering in the population is most consistent with subject-specific clustering for voxels involved in the experimental paradigm. The highest Dice score (0.725, for K=7) for *Signal* stays consistent across different model sizes. Clustering in the *PCA-Signal* space offers no noticeable improvement overworking with raw signals. Initial alignment of the diffusion maps into the *Linear-Atlas* substantially increases the Dice score of the highest ranked clusters for all values of model size *K*, with a maximum value of 0.876. The variational EM algorithm performed using a range of reasonable cluster numbers further improves the cluster agreement for the top ranked clusters (0.905).

Fig. 5 shows the networks that correspond to the top ranked atlas cluster (for $K = 10$), together with the corresponding average fMRI signal for all subjects in the study. Our method recovered the paradigm accurately, and for most subjects the cluster network plausibly spans visual, motor, and language areas. For subject 5 the corresponding cluster is substantially smaller. For this subject motion was higher than for all other subjects and was not entirely eliminated by the motion correction step. The language activation exhibited high scatter across the cortex compared to all other subjects. Fig. 6 compares the location and average signal of the top ranked cluster for $K = 10$ for *Signal* and *Atlas* models in a single subject. While both recover parts of the paradigm, the clustering in the atlas space is more consistent between the group and the subject levels. Additionally, the cluster in the signal space suffers from a relatively high dispersion across the entire cortex. This is not the case for the proposed functional atlas. The correlation between the average cluster signal and the paradigm increases slightly from 0.75 to 0.77, with the average absolute deviation decreasing from 0.84 to 0.80. The stability of the ICA components was below the one for the proposed methods, and never exceeded 0.2. In summary, these results demonstrate that the representation of fMRI time courses in the low dimensional space of diffusion maps captures the functional connectivity patterns across subjects better than the original space of signals. Not only are clustering assignments more consistent, but the spatial characteristics of these clusters are also more plausible anatomically. Furthermore, our results suggest that the probabilistic population model further improves the consistency across the population, and consolidates the distribution in the embedding space.

Transferring activation via the atlas

Fig. 7 illustrates the label transfer from the atlas population to new fMRI data. Figs. 8 and 9 report the accuracy of predicting activated regions by transferring features from the atlas to a single target subject. The plots show the overlap between the predicted region and the regions identified by a GLM detector on the target subject. We vary the p-value threshold in the GLM detector used in all subjects to evaluate the agreement between the atlas and individual subjects for a range of detection sensitivity settings. To account for different numbers of suprathreshold voxels on group-level and subject-specific maps, we determine the number based on the group-level p-value, and match an equal number of the lowest p-value voxels in the individuals. This results in the same number of voxels in the predictor (atlas) and the target (individual subject). Fig. 8 reports results of predicting the activation in a healthy subject that is part of the atlas population from activations in the $N - 1$ remaining

subjects of the atlas population. The matching accuracy within the atlas is substantially better for the functional registration compared to the anatomical atlas. This improvement is particularly strong for low thresholds, which correspond to signals that exhibit very strong activation for the fMRI experiment. The strong signals form relatively compact clusters in the map, leading to stable correspondences across subjects. To illustrate the improvement in accuracy for individual subjects, Fig. 8(b) reports subject-specific differences between functional and anatomical alignment, where positive values indicate higher overlap for functional alignment. All experiments were performed once using the inter-subject fMRI signal correlation as a basis for initial orthonormal alignment (red lines), or the spatial distance after registration to a joint template space (MNI) (cyan lines). In the latter case no inter-subject signal correlation is used at any point in the registration process. Orthonormal initialization based on fRMI signal correlation consistently leads to the highest overlap (red), while initialization based on spatial distance in the MNI space yields intermediate values (cyan). A leave-one-out cross validation (Figs. 8(c) and (d)) yields comparable results. Here the atlas is built from five control subjects, and the activations are transferred to the remaining subject as described in the Interpreting new data with help of the atlas section.

Fig. 9 reports the results of predicting activations in tumor patients using an atlas constructed on healthy control subjects, analogously to Fig. 8(c, d). Registration and atlas based grey matter segmentation yield results comparable to the healthy cohort on the tumor patients. Tumor tissue is typically partially segmented as grey matter, and was included as part of the potential target voxel set. All voxels classified as grey matter voxels are the target set in which activation is evaluated in the individual, and predicted by anatomical and functional alignment. This ensures consistent evaluation of the approaches, despite potential segmentation inaccuracies in the tumor neighborhood. When mapping active regions to tumor patients, the performance drops compared to the healthy atlas subjects. However, the functional atlas still outperforms the anatomical atlas in most cases, suggesting meaningful correspondences between atlas regions and those in the target image, despite pathology. The anatomical atlas registration leads to comparable results in subjects and patients. The median overlap for both cohorts is 0.21 for the lowest p-cutoff. The mean overlaps differ due to two outliers, subject 5 in the control cohort has low overlap (0.04), and patient 4 particularly high overlap (0.47).

Discussion

Alignment is a fundamental part of many neuroimaging studies. It is a prerequisite for comparing features such as brain activity at corresponding locations across subjects. However, in this context correspondence is ambiguous, since it can refer to appearance, anatomy, function, or even experimental condition. A widely accepted approach is to assume that once anatomical correspondence is established by registering anatomical MRI data, we can study function in populations, and obtain valid observations of its common characteristics and their variability. In this case variability of the spatial distribution of functional areas and their actual behavior are studied only jointly. If we aim to investigate spatial characteristics of functional areas (e.g., reorganization in tumor subjects), or functional characteristics of areas that exhibit location differences across individuals we have to find other means to establish correspondence. Even the assumption that

correspondences can be translated into a spatial mapping between subjects can be challenged. Functional correspondence can be a function of experimental condition, and regions that are recruited by different tasks might overlap for one subject, but not for another. For example, in some patients, initially unrelated areas are recruited for new functionality during reorganization (Duffau et al., 2001).

We propose and demonstrate a method to align functional MRI data across subjects based on their global functional connectivity patterns during a specific task. The experimental results demonstrate that this alignment is feasible and that it matches functionally corresponding regions more accurately than anatomical alignment in both healthy subjects and patients with mass lesions.

The underlying embedding and clustering in the embedding space are closely related to various approaches that have been employed for structure identification in fMRI data. (Thirion and Faugeras, 2004) demonstrated that non-linear embedding could be used to identify structure in subject-specific fMRI data. Group-level clusters in the embedding space, that rely on spatial correspondence across subjects have been investigated in Craddock et al. (2012). In contrast to these approaches, the proposed *functional connectivity alignment* uses the structure represented in the embedding space not only to characterize subjects, but also to establish correspondence across subjects irrespective of anatomical space. The results illustrate the extent to which embedding maps of multiple individual subjects exhibit sufficient common structure to match functional regions across the population, without assuming correspondence in the anatomical space.

Group alignment aims to form a joint representation that captures common characteristics of a population, while at the same time representing the individual data faithfully. For the proposed functional atlas this means that the point distribution that forms the map in the joint embedding space should accurately reflect the individual subject distributions, as the cluster agreement in our experiments indicates. In the first experiment, we observe that the structure of the joint distribution in the atlas is very similar to the structure in each individual subject map. That is, it captures the individual connectivity characteristics well, and matches them accurately across the population. We also observe that the alignment performs particularly well for brain areas that are active or interacting during fMRI acquisition. The signals from those areas forma distribution in the embedding space whose structure is repeated across subjects. Areas that do not exhibit connectivity captured by the correlation matrix are not matched well across subjects. The alignment is therefore specific for different experimental conditions. Resting state data would offer a potential alternative basis for alignment, since its correlation structure would cover the brain more evenly rather than highlight dominant networks (Sepulcre et al., 2010). Future work will focus on the role of resting state networks as a basis for alignment, and their complementary role to networks detected from task data.

In the second experiment, we evaluated whether the alignment establishes robust correspondences between areas that are active during the same task. The comparison shows that in a healthy cohort, functional alignment based on connectivity matches language areas with higher accuracy than anatomical alignment. This result holds regardless of whether

inter-subject fMRI signal correlations or anatomical registration is used for initialization. In both cases, the task information is not used explicitly by the alignment. However, in the first case high signal correlation of activated areas across subjects potentially drives successful registration. In the second case no signal correlation is used across subjects and the improvement over anatomical registration is due to the fact that the signal structure within the subjects offers sufficient similarity to enable matching. The proposed functional representation can therefore serve as a basis for registration in a way that is complementary to anatomical data. Our results support the use of functional connectivity alignment during neuroimaging studies in healthy subjects, since it could alleviate the degradation of group analysis by spatial variability of functional areas.

When using an atlas built based on a healthy cohort to localize language areas in patients who are not part of the atlas population, there is also improvement over anatomical registration. However, it is less pronounced than that for healthy subjects. For a more in-depth analysis a larger cohort with controlled tumor characteristics is necessary. At this point results demonstrate the feasibility of the proposed approach for patients, but do not allow deriving conclusions regarding the differences between the two cohorts.

The orthonormal alignment results in well matched maps, and the cluster agreement is already substantially better compared to mere signal clustering, clustering in a PCA signal space, or ICA. Non-linear alignment brings additional improvement. The non-linear alignment by variational EM estimates both the joint distribution, and the positions of the embedded points. The initial distribution is dominated by the relatively compact clusters of the individual subjects, which are misaligned across the population. In some cases this leads to early convergence without the correct identification of clusters across subjects, since the subject-specific clusters warrant relatively accurate approximation by the Gaussian distributions. In other words, the algorithm is too confident during the initial iterations, and consequently does not change point positions. Artificially increasing noise variance σ_s during this initial phase alleviated this problem, and allowed individual clusters to merge across subjects.

This work has several limitations. While we demonstrate the feasibility of the approach on both healthy controls and patients, we do not make any observation regarding actual reorganization patterns or their relationship to specific lesion types, or locations at this point. The small tumor cohort with relatively heterogeneous lesion types does not allow us to make conclusions regarding common characteristics in tumor patients whose language areas are affected, or a systematic comparison of the algorithms applied to healthy subjects and tumor patients. Instead, the results prove that functional connectivity alignment is feasible for both healthy subjects and tumor patients, and that It might be a good approach to tackle the question of correspondence in related future studies. The anatomical alignment was performed based on anatomical data and a corresponding MNI template using FSL (Woolrich et al., 2009) since this is a widely used approach. We note that there are alternatives such as the SPM DARTEL toolbox that establish a population specific anatomical template (Ashburner, 2009) that can improve registration performance in normal control subjects (Klein et al., 2009). However, generating a population specific template from patients affected by tumors is not straightforward. To make results on patients and

control subjects comparable, we used a standard template for both. Further alternatives would be surface based registration such as the approach implemented in FreeSurfer (Fischl et al., 2002), and cortical profile registration (Sabuncu et al., 2010a). We validated if the captured correspondences are meaningful and not an arbitrary match of signals by comparing the overlap of areas activated by the language paradigm. Paradigm information is not available to the alignment algorithm. Repeating alignment on repeated scans of the same individuals to validate stability was not performed since data was not available. The embedding map is based on correlation among fMRI signals. There are several potential causes for high correlation unrelated to neural activity such as motion or susceptibility artifacts. Similarly to studies that focus on resting state fMRI, the results are expected to improve if these factors are accounted for by measures such as outlier detection (Jo et al., 2010), or noise correction (Behzadi et al., 2007). The embedding is based on a thresholded matrix. Although this is in line with related work (Varoquaux et al., 2010; Supekar et al., 2008), we note that negative correlation is lost. Including negative correlations is likely to improve segmentations for structures such as the default network. Worsley et al. (2005) offer a discussion of the impact of thresholding in functional network analysis.

Alignment based on functional connectivity patterns offers an approach to formulate and tackle various open questions that are beyond the scope of this paper. The decoupling of functional characteristics and location makes it possible to observe and quantify the relationship between spatial distribution of regions and their functional role. It enables the study of networks observed during different experimental conditions, and offers alignment of subject data in group studies that reduces variability introduced by anatomy. When comparing functional characteristics across cohorts, it separates anatomical variability, and functional differences. Ultimately it can serve as a tool to study the reorganization of networks and its relationship to function recovery.

Conclusions

We propose a method to learn an atlas of the functional connectivity structure that emerges during a cognitive process observed in a group of individuals. The atlas is a groupwise generative model that describes the fMRI responses of all subjects in the embedding space. The embedding space is a low dimensional representation of fMRI time courses that encodes the functional connectivity patterns within each subject. Results from an fMRI language experiment indicate that the diffusion map framework captures the connectivity structure reliably, and leads to valid correspondences across subjects. Future work will focus on the application of the framework to study reorganization processes.

Acknowledgments

This work was funded in part by the NSF IIS/CRCNS 0904625 grant, the NSF CAREER 0642971 grant, NIH NCRR NAC P41-RR13218 and NIH NIBIB NAC P41-EB-015902, NIH NIBIB NAMIC U54-EB005149, NIH U41RR019703, NIH NICHD R01HD067312, and NIH P01CA067165 grants, the Brain Science Foundation, the Klarman Family Foundation, EU (FP7/2007–2013) n°257528 (KHRESMOI) and no 330003 (FABRIC), Austrian Science Fund no P 22578-B19 (PULMARCH). We would like to thank Veronika Schöpf for helpful discussions.

Appendix A. Diffusion map coordinates

In the standard diffusion map analysis, the embedding coordinates $\mathbf{\Gamma}$ for a L-dimensional space are obtained via the first L eigenvectors of matrix $\mathbf{A} = \mathbf{D}^{-1/2}\mathbf{W}\mathbf{D}^{-1/2}$ (Nadler et al., 2007). Here we show that we can represent the embedding as a solution of a least-squares problem formulated directly on the similarity matrix $\mathbf{W}$.

Formally, $\mathbf{\Gamma}=\mathbf{D}^{-1/2}\mathbf{V}_{1:L}\mathbf{\Lambda}_L^t$, where $\mathbf{A} = \mathbf{V}\mathbf{\Lambda}\mathbf{V}^T$ is the eigenvector decomposition of matrix $\mathbf{A}$, t is the diffusion time, and subscripts 1: L indicate that we select the first L eigenvectors. $\mathbf{V}_{1:L}$ is a $N \times L$ matrix, $\mathbf{\Lambda}_L$ is a $L \times L$ diagonal matrix of the first eigenvalues. Matrix $\tilde{\mathbf{A}}=\mathbf{V}_{1:L}\mathbf{\Lambda}_L\mathbf{V}_{1:L}^T$ is a low-rank approximation of matrix $\mathbf{A}$ that is quite accurate if the remaining eigenvalues are much smaller than the sum of the first L eigenvalues. We define

$$\mathbf{L}=\mathbf{D}^{-1/2}\mathbf{A}^{2t}\mathbf{D}^{-1/2} \approx \mathbf{D}^{-1/2}\tilde{\mathbf{A}}^{2t}\mathbf{D}^{-1/2}=\mathbf{D}^{-1/2}\left(\mathbf{V}_{1:L}\Lambda_L\mathbf{V}_{1:L}^T\right)^{2t}\mathbf{D}^{-1/2} =\mathbf{D}^{-1/2}\mathbf{V}_{1:L}\Lambda_L^t\Lambda_L^t\mathbf{V}_{1:L}^T\mathbf{D}^{-1/2}=\mathbf{\Gamma}\mathbf{\Gamma}^T, \quad \text{(A.1)}$$

and use a generalization of the Eckart–Young theorem (Friedland and Torokhti, 2006) to formulate the eigen decomposition as an optimization problem:

$$\mathbf{\Gamma}^*=\underset{\Gamma\in\mathbb{R}^{N\times L}}{\operatorname{argmin}}\left\|\mathbf{A}^2-\mathbf{D}^{1/2}\mathbf{\Gamma}\mathbf{\Gamma}^T\mathbf{D}^{1/2}\right\|_F^2=\underset{\Gamma\in\mathbb{R}^{N\times L}}{\operatorname{argmin}}\sum_{i,j}d_id_j\left(\mathbf{L}_t(i,j)-\gamma_i^T\gamma_j\right)^2, \quad \text{(A.2)}$$

where $\|\cdot\|_F$ denotes the Frobenius norm.

Appendix B. Variational EM update rules

We use a natural choice of a multinomial distribution for cluster membership $q(z_{si} = k)$ for $s \in \{1, \ldots, S\}$, $i \in \{1, \ldots, N_s\}$, and a Gaussian distribution for the embedding coordinates $q(\gamma_{si}) = \mathcal{N}(\gamma_{si}; \mathbb{E}\gamma_{si}], \operatorname{diag}(\mathbb{V}\gamma_{si}]))$, parameterized by its mean $\mathbb{E}\gamma_{si}]$ and component-wise variance $\mathbb{V}\gamma_{si}]$.

B.1. E-Step

We determine the parameter values of the approximating probability distribution $q(\cdot)$ that minimize the Gibbs free energy in Eq. (9) by evaluating the expectation, differentiating with respect to each parameter and setting the derivatives to zero. This yields

$$q(z_{si}=k) \propto \frac{\pi_k}{|\Theta_k|^{1/2}}\exp\left\{-\frac{1}{2}\left((\mathbb{E}[\gamma_{si}]-\mu_k)^T\Theta_k^{-1}(\mathbb{E}[\gamma_{si}]-\mu_k)+\operatorname{trace}\left(\operatorname{diag}(\mathbb{V}[\gamma_{si}])\Theta_k^{-1}\right)\right)\right\}, \text{s.t}\sum_k q(z_{si}=k)=1,$$

$$\mathbb{V}[\gamma_{si}(l)]=\left(\sum_k q(z_{si}=k)\Theta_k^{-1}(l,l)+\frac{d_{si}}{\sigma_s^2}\sum_{j\neq i}d_{sj}\left(\mathbb{E}[\gamma_{sj}(l)]^2+\mathbb{V}\left[\gamma_{sj}(l)\right]\right)\right)^{-1},$$

$$\begin{aligned}
&\mathbb{E}[\gamma_{si}(l)] \\
&\quad = \mathbb{V}[\gamma_{si}(l)] \left[\sum_k q(z_{si} \right. \\
&\qquad = k) \left[\Theta_k^{-1}(l,l)\mu_k(l) \right. \\
&\qquad - \sum_{l' \neq l} \Theta_k^{-1}(l,l')(\mathbb{E}[\gamma_{si}(l') \\
&\qquad\quad - \mu_k(l'))] \\
&\qquad + \frac{d_{si}}{\sigma_s^2} \sum_{j \neq i} d_{sj} \left[\mathbf{L}_s(i,j)\mathbb{E}\left[\gamma_{sj}(l)\right] \right. \\
&\qquad\quad \left. \left. - \mathbb{E}\left[\gamma_{sj}(l)\right] \sum_{l' \neq l} \mathbb{E}[\gamma_{si}(l')]\mathbb{E}\left[\gamma_{sj}(l')\right] \right] \right] .
\end{aligned}$$

Rather than solve the coupled system of equations above, we iteratively update each parameter of the distribution $q(\cdot)$ while fixing all the other parameters.

B.2. M-Step

We now find the parameter values with the update rules that are similar to the standard EM algorithm for mixture modeling, but using the approximating distribution $q(\cdot)$ to evaluate the expectation. Specifically, we find

$$\pi_k = \frac{1}{\sum_s N_s} \sum_{s,i} q(z_i = k), \quad \text{(B.1)}$$

$$\mu_k = \sum_{s,i} \frac{q(z_{si} = k)}{\sum_{s'l'} q(z_{s'i'} = k)} \mathbb{E}[\gamma_{si}], \quad \text{(B.2)}$$

$$\Theta_k = \sum_{s,i} \frac{q(z_{si} = k)}{\sum_{s,'i'} q(z_{s'i'} = k)} \left[(\mathbb{E}[\gamma_{si}] - \mu_k)(\mathbb{E}[\gamma_{si}] - \mu_k)^T + \mathrm{diag}(\mathbb{V}[\gamma_{si}]) \right], \quad \text{(B.3)}$$

$$\sigma_s^2 = \frac{2}{N_s(N_s - 1)} \sum_{i,j \neq i} d_{si} d_{sj} \mathbb{E}\left[\left(\mathbf{L}_s(i,j) - \gamma_{si}^T \gamma_{sj} \right)^2 \right] . \quad \text{(B.4)}$$

Appendix C. Patient information

Table 1

Information on the patients. All patients were right-handed according to the Edinburgh Handedness Inventory.

No.	Gender/ Age	Diagnosis	Tumor location/Size (cm^3)	Clinical language function assessment		Intra-operative language mapping	
				Pre-op	Post-op	Technique	Results
1	M/43	Ganglioglioma WHO Grades I–II	Left temp/2.91	Normal	Normal	Wada test	Left hemisphere dominance for language
2	F/55	Metastatic adenocarcinoma	Left temporal/7.58	Normal	Normal	ECS testing	Left hemisphere involvement of language
3	F/30	Glioblastoma WHO Grade IV	Left temporal/38.42	Speech difficulty	Better	ECS testing	Tumor surrounding areas involvement of language
4	M/50	Anaplastic oligoastrocytoma WHO Grade III	Left temporal/7.27	Occasional word finding difficulty	Occasional word finding difficulty to normal	ECS testing	Language areas were in the left hemisphere, and posterior to lesion
5	F/66	Metastatic adenocarcinoma	Left parietal/1.67; left temporal/0.20	Normal	Normal	ECS testing	No critical language areas immediately adjacent to lesion
6	M/35	Oligoastrocytoma WHO Grade II	Left frontal/19.62	Normal	Normal	N/a	N/a
7	F/57	Glioblastoma WHO Grade IV	Left temporal/8.59	Speech difficulty	N/a	ECS testing	No critical language areas in the region of lesion

References

Ackermann H, Riecker A. The contribution of the insula to motor aspects of speech production: a review and a hypothesis. Brain Lang. 2004; 89:320–328. http://dx.doi.org/10.1016/S0093-934X(03)00347-X. [PubMed: 15068914]

Ashburner J. Computational anatomy with the SPM software. Magn. Reson. Imaging. 2009; 27:1163–1174. [PubMed: 19249168]

Behzadi Y, Restom K, Liau J, Liu TT. A component based noise correction method (CompCor) for BOLD and perfusion based fMRI. Neuroimage. 2007; 37:90–101. [PubMed: 17560126]

Buckner RL, Andrews-Hanna JR, Schacter DL. The brain's default network: anatomy, function, and relevance to disease. Ann. N. Y. Acad. Sci. 2008; 1124:1–38. http://dx.doi.org/10.1196/annals.1440.011. [PubMed: 18400922]

Coifman RR, Lafon S. Diffusion maps. Appl. Comput. Harmon. Anal. 2006; 21:5–30.

Collins D, Holmes C, Peters T, Evans A. Automatic 3-d model-based neuroanatomical segmentation. Hum. Brain Mapp. 1995; 3:190–208.

Craddock RC, James GA, Holtzheimer PE, Hu XP, Mayberg HS. A whole brain fMRI atlas generated via spatially constrained spectral clustering. Hum. Brain Mapp. 2012; 33:1914–1928. [PubMed: 21769991]

Davis BC, Fletcher PT, Bullitt E, Joshi S. Population shape regression from random design data. Int. J. Comput. Vis. 2010; 90:255–266.

Desmurget M, Bonnetblanc F, Duffau H. Contrasting acute and slow-growing lesions: a new door to brain plasticity. Brain. 2007; 130:898–914. http://dx.doi.org/10.1093/brain/awl300. [PubMed: 17121742]

Dice LR. Measures of the amount of ecologic association between species. Ecology. 1945; 26:297–302.

Dittrich E, Riklin Raviv T, Kasprian G, Donner R, Brugger PC, Prayer D, Langs G. A spatio-temporal latent atlas for semi-supervised learning of fetal brain segmentations and morphological age estimation. Med. Image Anal. 2014; 18:9–21. http://dx.doi.org/10.1016/j.media.2013.08.004. [PubMed: 24080527]

Duffau H, Bauchet L, Lehéricy S, Capelle L. Functional compensation of the left dominant insula for language. Neuroreport. 2001; 12:2159–2163. [PubMed: 11447326]

Elbert T, Rockstroh B. Reorganization of human cerebral cortex: the range of changes following use and injury. Neuroscientist. 2004; 10:129–141. http://dx.doi.org/10.1177/1073858403262111. [PubMed: 15070487]

Elkana O, Frost R, Kramer U, Ben-Bashat D, Hendler T, Schmidt D, Schweiger A. Cerebral reorganization as a function of linguistic recovery in children: an fMRI study. Cortex. 2009 http://dx.doi.org/10.1016/j.cortex.2009.12.003.

Erhardt EB, Rachakonda S, Bedrick EJ, Allen EA, Adali T, Calhoun VD. Comparison of multi-subject ICA methods for analysis of fMRI data. Hum. Brain Mapp. 2011; 32:2075–2095. [PubMed: 21162045]

Fedorenko E, Kanwisher N. Some regions within broca's area do respond more strongly to sentences than to linguistically degraded stimuli: a comment on Rogalsky and Hickok (2011). J. Cogn. Neurosci. 2011; 23:2632–2635.

Fedorenko E, Hsieh PJ, Nieto-Castañón A, Whitfield-Gabrieli S, Kanwisher N. New method for fMRI investigations of language: defining ROIs functionally in individual subjects. J. Neurophysiol. 2010; 104:1177–1194. http://dx.doi.org/10.1152/jn.00032.2010. [PubMed: 20410363]

Fischl B, Salat D, Busa E, Albert M, Dieterich M, Haselgrove C, van der Kouwe A, Killiany R, Kennedy D, Klaveness S, et al. Whole brain segmentation: automated labeling of neuroanatomical structures in the human brain. Neuron. 2002; 33:341–355. [PubMed: 11832223]

Friedland S, Torokhti A. Generalized Rank-Constrained Matrix Approximations, (Arxiv preprint math/0603674). 2006

Friston K, Holmes A, Worsley K, Poline J, Frith C, Frackowiak R, et al. Statistical parametric maps in functional imaging: a general linear approach. Hum. Brain Mapp. 1995; 2:189–210. (URL: http://doi.wiley.com/10.1002/hbm.460020402).

Friston K, Frith C, Fletcher P, Liddle P, Frackowiak R. Functional topography: multidimensional scaling and functional connectivity in the brain. Cereb. Cortex. 1996; 6:156. [PubMed: 8670646]

Hagmann P, Cammoun L, Gigandet X, Meuli R, Honey CJ, Wedeen VJ, Sporns O, Friston KJ. Mapping the structural core of human cerebral cortex. Plos Biol. 2008; 6:e159. http://dx.doi.org/10.1371/journal.pbio.0060159. [PubMed: 18597554]

Haxby J, Guntupalli J, Connolly A, Halchenko Y, Conroy B, Gobbini M, Hanke M, Ramadge P. A common, high-dimensional model of the representational space in human ventral temporal cortex. Neuron. 2011; 72:404–416. [PubMed: 22017997]

He Y, Wang J, Wang L, Chen ZJ, Yan C, Yang H, Tang H, Zhu C, Gong Q, Zang Y, Evans AC. Uncovering intrinsic modular organization of spontaneous brain activity in humans. PLoS One. 2009; 4:e5226. [PubMed: 19381298]

Heiss WD, Thiel A, Kessler J, Herholz K. Disturbance and recovery of language function: correlates in pet activation studies. Neuroimage. 2003; 20(Suppl. 1):S42–S49. [PubMed: 14597295]

Jaakkola T. Tutorial on Variational Approximation Methods. Advanced Mean Field Methods: Theory and Practice. 2000:129–159.

Jo HJ, Saad ZS, Simmons WK, Milbury LA, Cox RW. Mapping sources of correlation in resting state FMRI, with artifact detection and removal. Neuroimage. 2010; 52:571–582. [PubMed: 20420926]

Klein A, Andersson J, Ardekani BA, Ashburner J, Avants B, Chiang MC, Christensen GE, Collins DL, Gee J, Hellier P, et al. Evaluation of 14 nonlinear deformation algorithms applied to human brain mri registration. Neuroimage. 2009; 46:786–802. [PubMed: 19195496]

Kuhl PK. Brain mechanisms in early language acquisition. Neuron. 2010; 67:713–727. http://dx.doi.org/10.1016/j.neuron.2010.08.038. [PubMed: 20826304]

Kveraga K, Ghuman AS, Kassam KS, Aminoff EA, Hämäläinen MS, Chaumon M, Bar M. Early onset of neural synchronization in the contextual associations network. Proc. Natl. Acad. Sci. U. S. A. 2011; 108:3389–3394. http://dx.doi.org/10.1073/pnas.1013760108. [PubMed: 21300869]

Lafon S, Lee A. Diffusion maps and coarse-graining: a unified framework for dimensionality reduction, graph partitioning, and data set parameterization. IEEE TPAMI. 2006:1393–1403.

Langs G, Samaras D, Paragios N, Honorio J, Alia-Klein N, Tomasi D, Volkow ND, Goldstein RZ. Task-specific functional brain geometry from model maps. Proc. of MICCAI. 2008:925–933.

Langs, G.; Tie, Y.; Rigolo, L.; Golby, A.; Golland, P. Functional geometry alignment and localization of brain areas. In: Lafferty, J.; Williams, CKI.; Shawe-Taylor, J.; Zemel, R.; Culotta, A., editors. Advances in Neural Information Processing Systems. 2010. p. 1225-1233.

Langs G, Lashkari D, Sweet A, Tie Y, Rigolo L, Golby AJ, Golland P. Learning an atlas of a cognitive process in its functional geometry. Inf. Process. Med. Imaging. 2011; 22:135–146. [PubMed: 21761652]

Lashkari D, Vul E, Kanwisher N, Golland P. Discovering structure in the space of fMRI selectivity profiles. Neuroimage. 2010; 50:1085–1098. [PubMed: 20053382]

Meila M, Shi J. A Random Walks View of Spectral Segmentation. AISTATS. 2001:1–6.

Meyer PT, Sturz L, Schreckenberger M, Spetzger U, Meyer GF, Setani KS, Sabri O, Buell U. Preoperative mapping of cortical language areas in adult brain tumour patients using pet and individual non-normalised SPM analyses. Eur. J. Nucl. Med. Mol. Imaging. 2003; 30:951–960. http://dx.doi.org/10.1007/s00259-003-1186-1. [PubMed: 12748833]

Mueller SG, Weiner MW, Thal LJ, Petersen RC, Jack CR, Jagust W, Trojanowski JQ, Toga AW, Beckett L. Ways toward an early diagnosis in Alzheimer's disease: the Alzheimer's disease neuroimaging initiative (ADNI). Alzheimers Dement. 2005; 1:55–66. http://dx.doi.org/10.1016/j.jalz.2005.06.003. [PubMed: 17476317]

Nadler B, Lafon S, Coifman R, Kevrekidis I. Diffusion maps — a probabilistic interpretation for spectral embedding and clustering algorithms. Principal Manifolds for Data Visualization and Dimension Reduction. 2007:238–260.

Rosales, R.; Frey, B. Learning generative models of affinity matrices; Proceedings of the 19th Annual Conference on Uncertainty in Artificial Intelligence (UAI-03); 2003. p. 485-492.

Sabuncu M, Singer B, Conroy B, Bryan R, Ramadge P, Haxby J, et al. Function-based intersubject alignment of human cortical anatomy. Cereb. Cortex. 2010a; 20:130–140. [PubMed: 19420007]

Sabuncu M, Yeo B, Van Leemput K, Fischl B, Golland P. A generative model for image segmentation based on label fusion. IEEE Trans. Med. Imaging. 2010b; 29:1714–1729. [PubMed: 20562040]

Saxe R, Brett M, Kanwisher N. Divide and conquer: a defense of functional localizers. Neuroimage. 2006; 30:1088–1096. [PubMed: 16635578]

Scholz J, Klein MC, Behrens TEJ, Johansen-Berg H. Training induces changes in white-matter architecture. Nat. Neurosci. 2009; 12:1370–1371. http://dx.doi.org/10.1038/nn.2412. [PubMed: 19820707]

Scott G, Longuet-Higgins H. An algorithm for associating the features of two images. Proc. Biol. Sci. 1991; 244:21–26. [PubMed: 1677192]

Sepulcre J, Liu H, Talukdar T, Martincorena I, Yeo BTT, Buckner RL. The organization of local and distant functional connectivity in the human brain. PLoS Comput. Biol. 2010; 6:e1000808. http://dx.doi.org/10.1371/journal.pcbi.1000808. [PubMed: 20548945]

Suarez R, Whalen S, O'Shea J, Golby A. A surgical planning method for functional MRI assessment of language dominance: influences from threshold, region-of-interest, and stimulus mode. Brain Imaging Behav. 2008; 2:59–73.

Supekar K, Menon V, Rubin D, Musen M, Greicius MD. Network analysis of intrinsic functional brain connectivity in Alzheimer's disease. PLoS Comput. Biol. 2008; 4:e1000100. [PubMed: 18584043]

Talairach, J.; Tournoux, P. Co-Planar Stereotaxic Atlas of the Human Brain. New York: Thieme; 1988.

Thirion, B.; Faugeras, O. Nonlinear dimension reduction of fMRI data: the Laplacian embedding approach; Biomedical Imaging: Nano to Macro, 2004. IEEE International Symposium on, IEEE; 2004. p. 372-375.

Thirion B, Dodel S, Poline JB. Detection of signal synchronizations in resting-state fmri datasets. Neuroimage. 2006; 29:321–327. http://dx.doi.org/10.1016/j.neuroimage.2005.06.054. [PubMed: 16129624]

Tie Y, Suarez R, Whalen S, Radmanesh A, Norton I, Golby A. Comparison of blocked and event-related fMRI designs for pre-surgical language mapping. Neuroimage. 2009; 47:107–115. [PubMed: 19361563]

Varoquaux, G.; Gramfort, A.; Poline, JB.; Thirion, B. Brain covariance selection: better individual functional connectivity models using population prior. In: Lafferty, J.; Williams, CKI.; Shawe-Taylor, J.; Zemel, R.; Culotta, A., editors. Advances in Neural Information Processing Systems. Vol. 23. 2010. p. 2334-2342.

Venkataraman A, Rathi Y, Kubicki M, Westin C, Golland P. Joint generative model for fMRI/DWI and its application to population studies. Medical Image Computing and Computer-Assisted Intervention — MICCAI. 2010; 2010:191–199.

Von Luxburg U. A tutorial on spectral clustering. Stat. Comput. 2007; 17:395–416.

Von Luxburg U, Radl A, Hein M. Getting lost in space: large sample analysis of the commute distance. Adv. Neural Inf. Process. Syst. 2010; 24:5.

Wolz R, Aljabar P, Hajnal JV, Loetjoenen J, Rueckert D. The Alzheimer's Disease Neuroimaging Initiative. Nonlinear dimensionality reduction combining MR imaging with non-imaging information. Med. Image Anal. 2011 http://dx.doi.org/10.1016/j.media.2011.12.003.

Woolrich MW, Jbabdi S, Patenaude B, Chappell M, Makni S, Behrens T, Beckmann C, Jenkinson M, Smith SM. Bayesian analysis of neuroimaging data in FSL. Neuroimage. 2009; 45:S173–S186. http://dx.doi.org/10.1016/j.neuroimage.2008.10.055. [PubMed: 19059349]

Worsley K, Chen JI, Lerch J, Evans A. Comparing functional connectivity via thresholding correlations and singular value decomposition. Philos. Trans. R. Soc. B-Biol. Sci. 2005; 360:913–920.

Yeo BTT, Sabuncu MR, Vercauteren T, Holt DJ, Amunts K, Zilles K, Golland P, Fischl B. Learning task-optimal registration cost functions for localizing cytoarchitecture and function in the cerebral cortex. IEEE Trans. Med. Imaging. 2010; 29:1424–1441. http://dx.doi.org/10.1109/TMI.2010.2049497. [PubMed: 20529736]

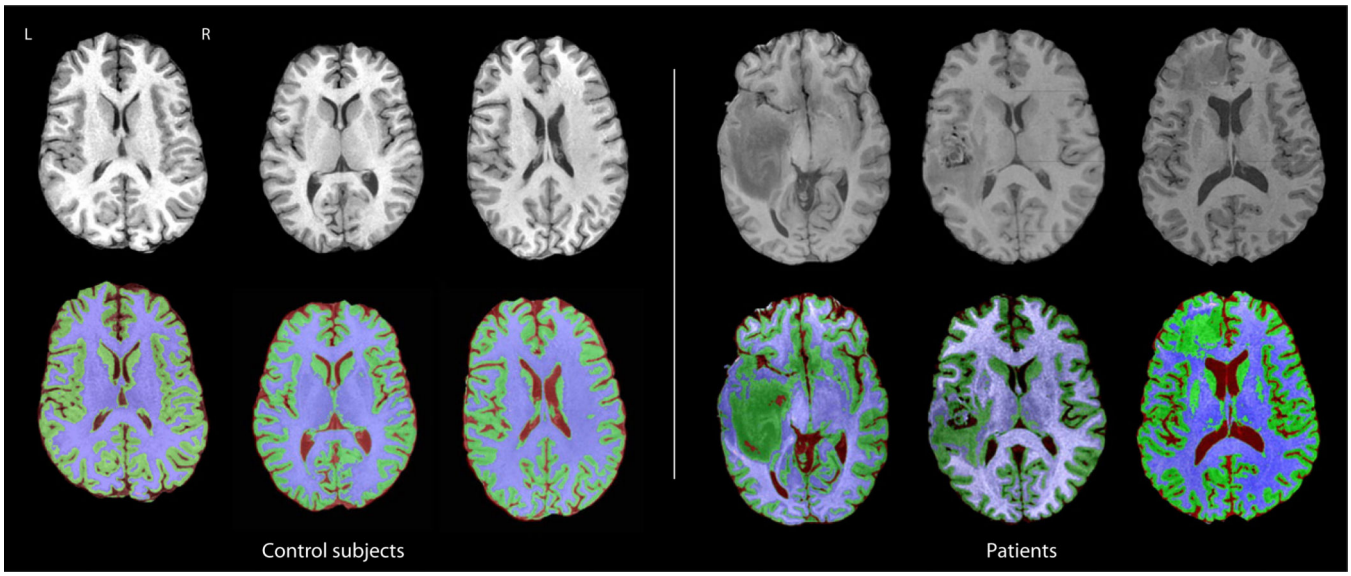

Figure 1.
Example axial MRI slice in three control subjects, and three tumor patients. For each we show the T1 MRI data and a corresponding FSL segmentation as described in the experiment section.

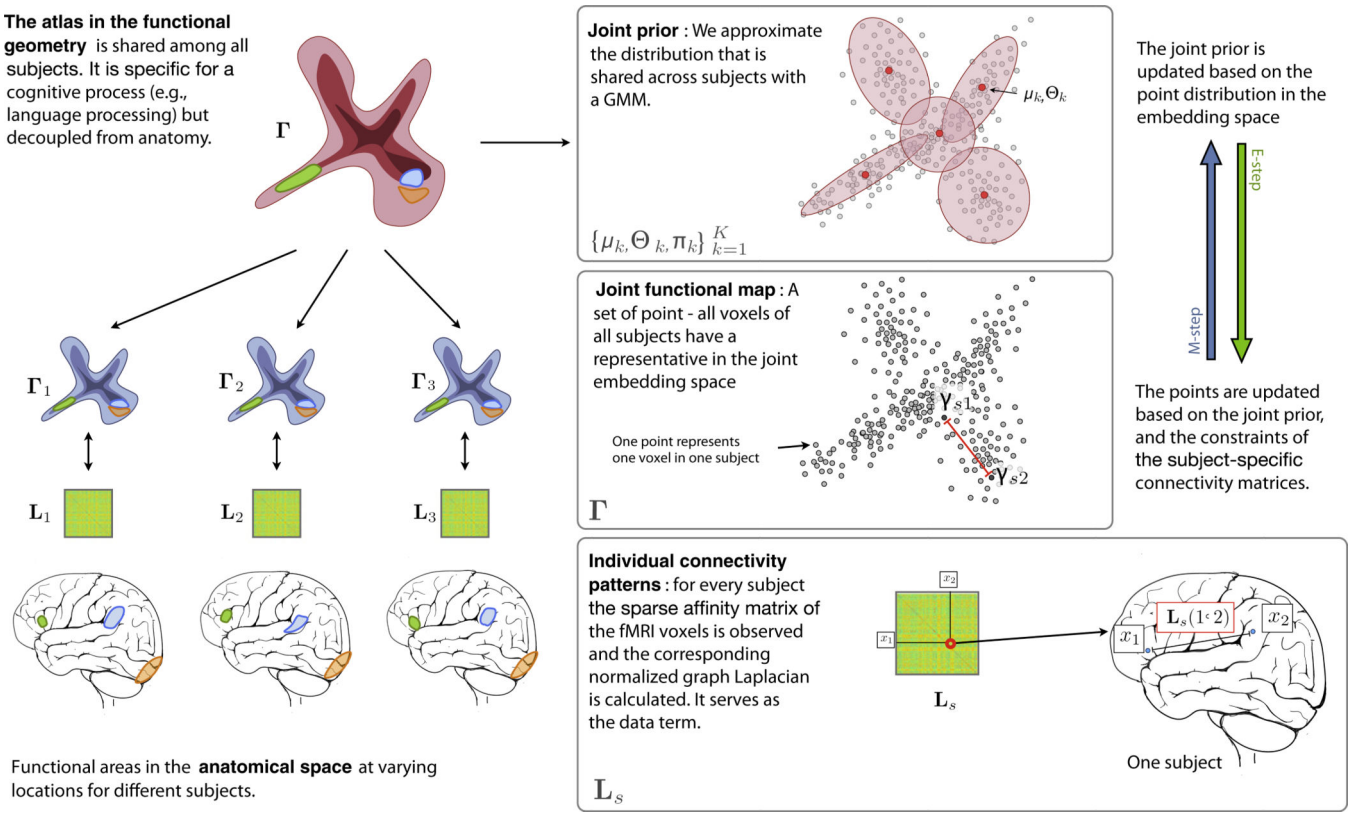

Figure 2.

Joint functional geometry. The atlas represents the functional connectivity structure observed in all subjects of the population. Each voxel in each subject is represented by a point in the joint distribution. The distribution parameters are shared across subjects. Parameters and embedding point positions are estimated via variational EM.

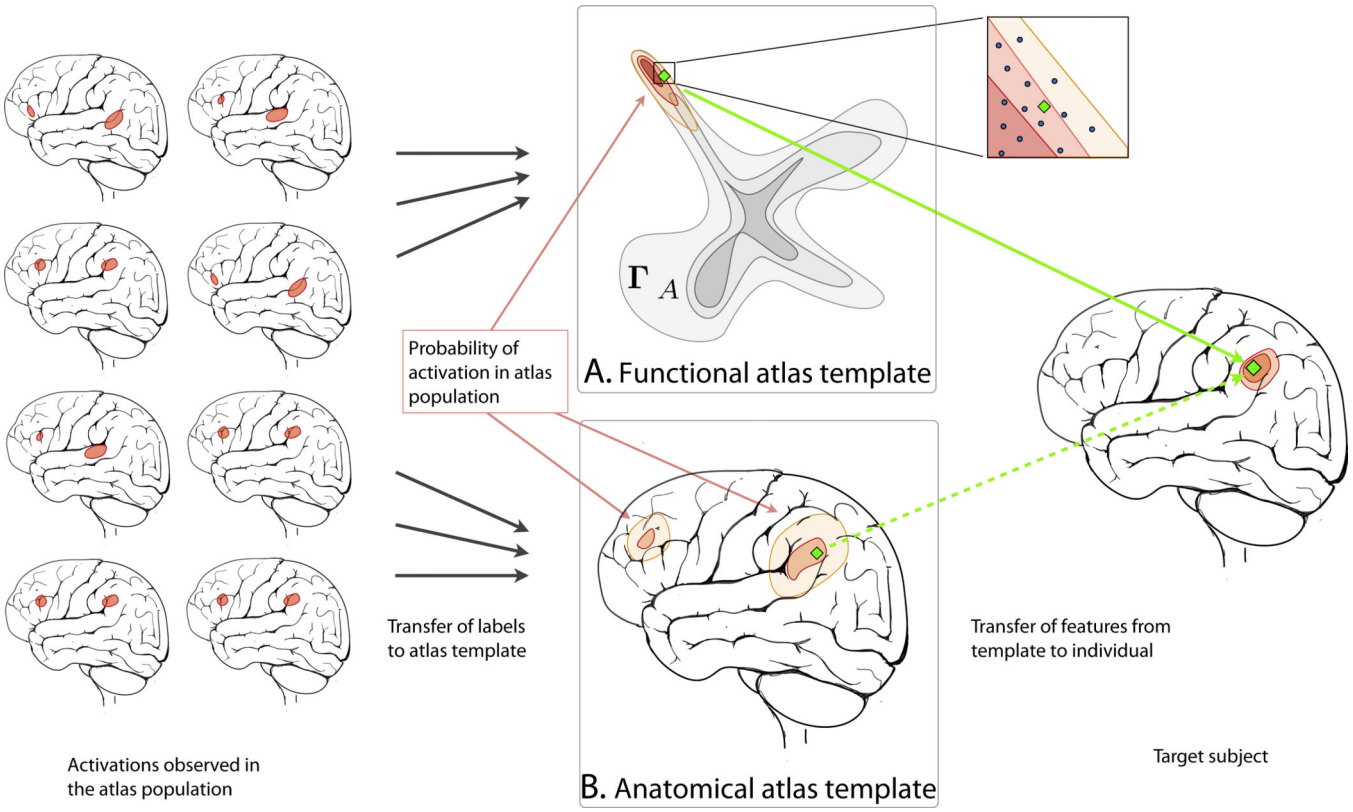

Figure 3.

Transferring labels from the atlas to an individual. In this example activation probabilities are collected for each position in the functional atlas (A), or in a standard anatomical atlas (B). They are then transferred to a new subject after aligning to the template (functional or anatomical). The anatomical template assumes tight coupling between space and function, the functional template does not.

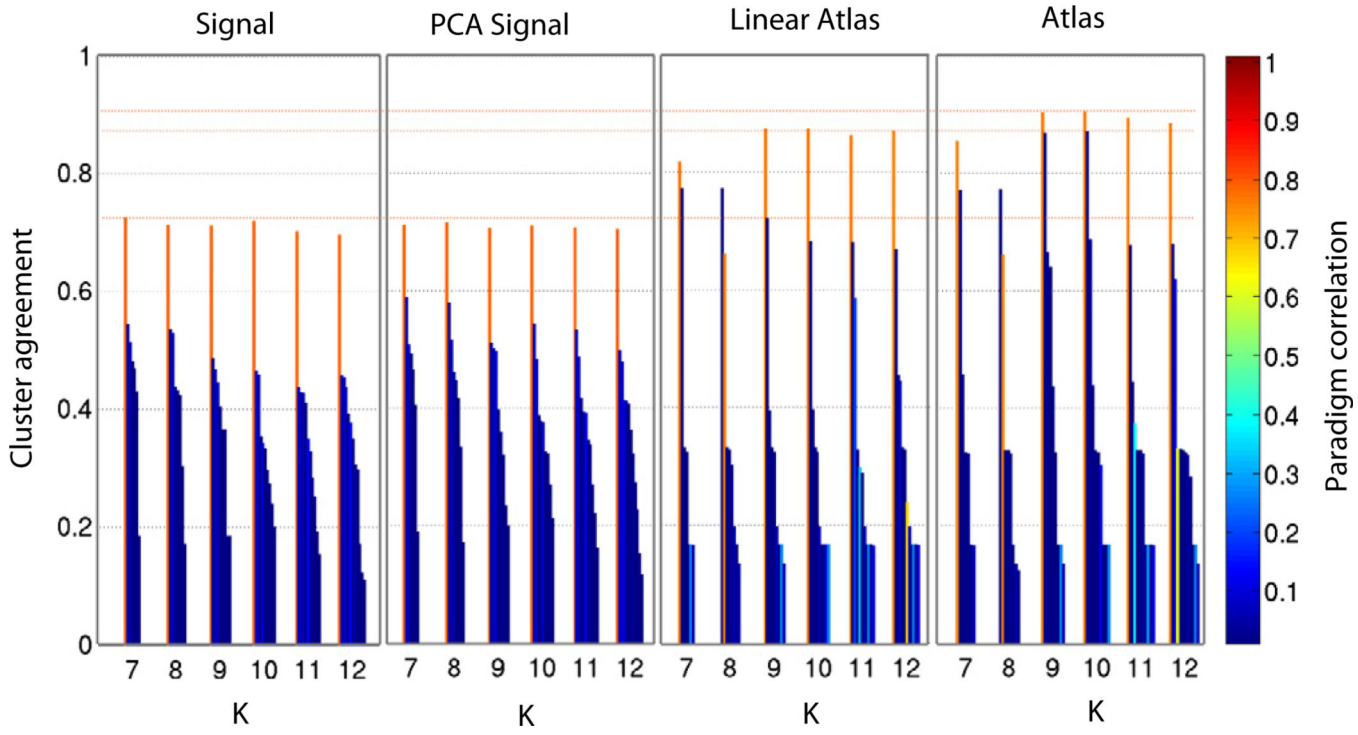

Figure 4.

Average cluster agreement between group-level and subject-specific clusters estimated from raw signals (*Signal*), signals after PCA (*PCA Signal*), embedding coordinates after linear alignment (*Linear Atlas*), and embedding coordinates after non-linear alignment by variational EM (*Atlas*). For each number of clusters *K*, we report the mean voxel set overlap between group-level and subject-specific clusters. To visualize the relationship of clusters with the language paradigm, color corresponds to the value of the correlation coefficient of the cluster average fMRI signal with the paradigm signal.

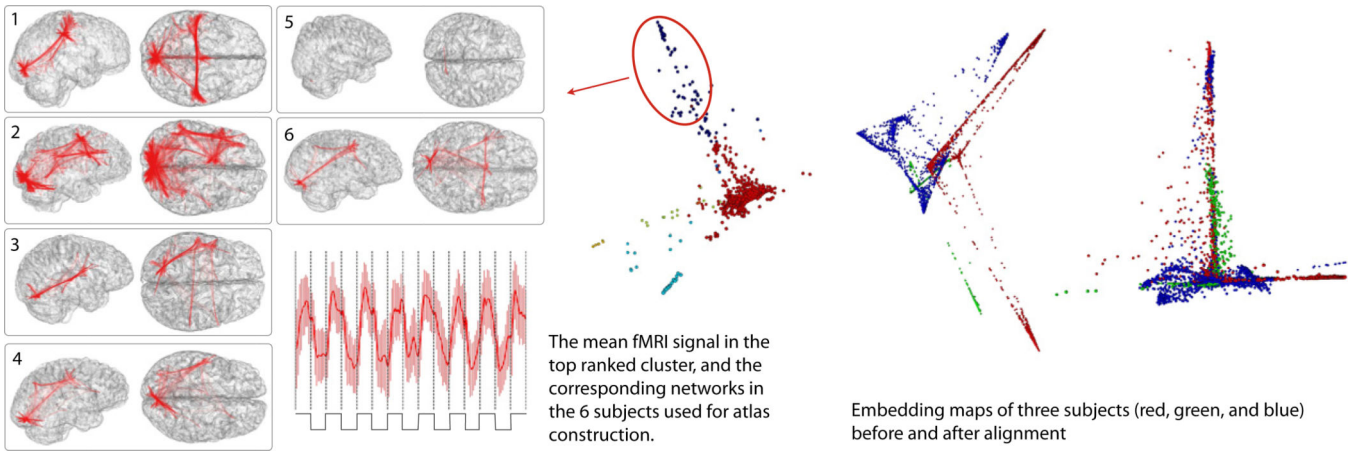

Figure 5.

A cluster in the joint map corresponds to a network in each subject. Here we illustrate a network that corresponds to one cluster in the atlas, and the mean fMRI signal of this cluster. While the 8-block paradigm in this language study was not explicitly used by the analysis, it is recovered by clustering. The right side of the figure shows the individual maps of three subjects before and after alignment in the embedding space (color corresponds to a subject).

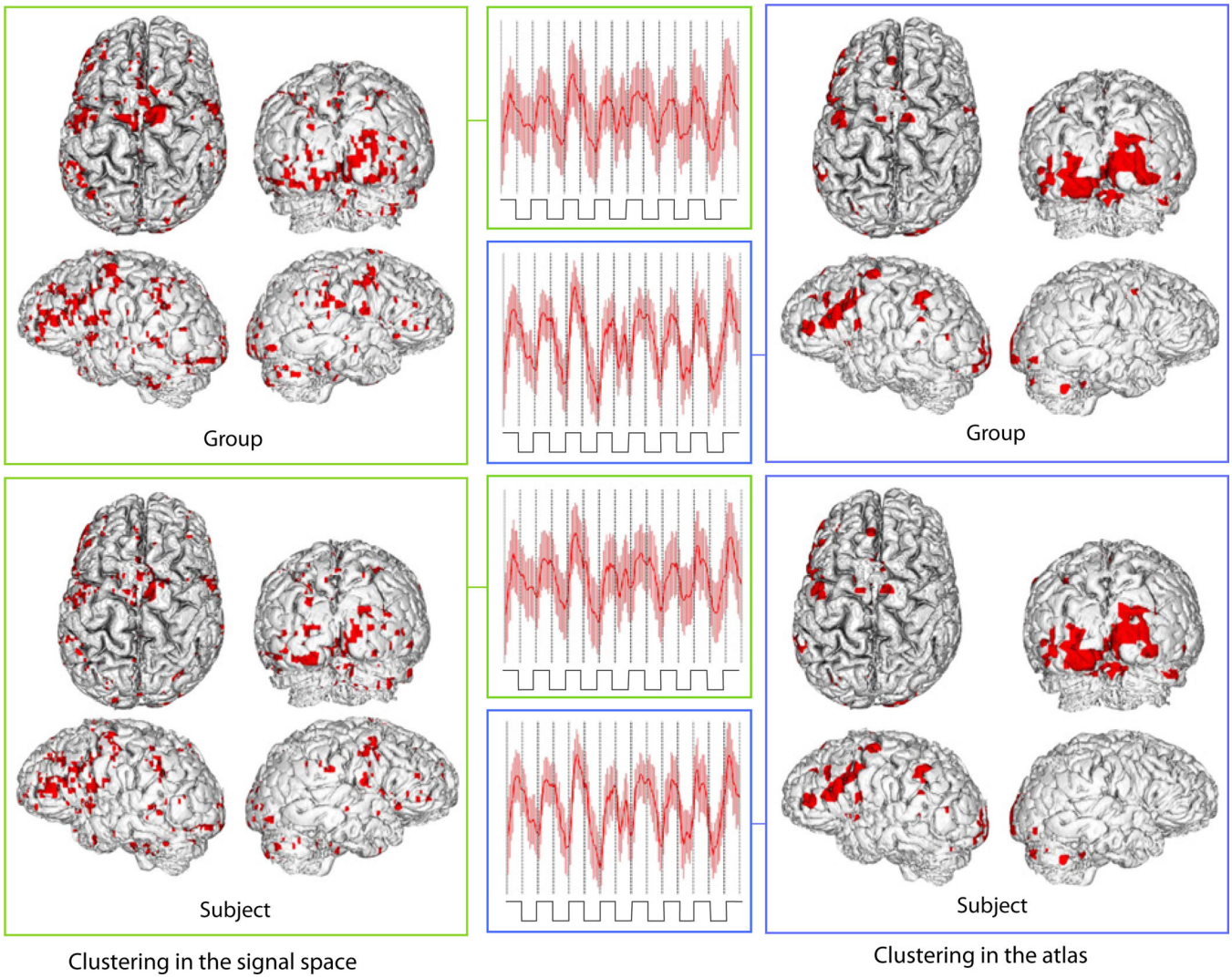

Figure 6.

The most consistent cluster in the *Signal* space and the *Atlas* space is shown in the anatomical space. The 8-block paradigm in this language study was not explicitly used by the analysis, but was recovered by the algorithm. The corresponding networks were identified across all subjects. They typically span the visual cortex, the language areas (Wernicke and Broca), and the motor areas in some cases. For each method, the group-wise (top) and subject-specific (bottom) assignment for subject 2 are displayed. Also shown is the average and standard deviation of the cluster fMRI signal.

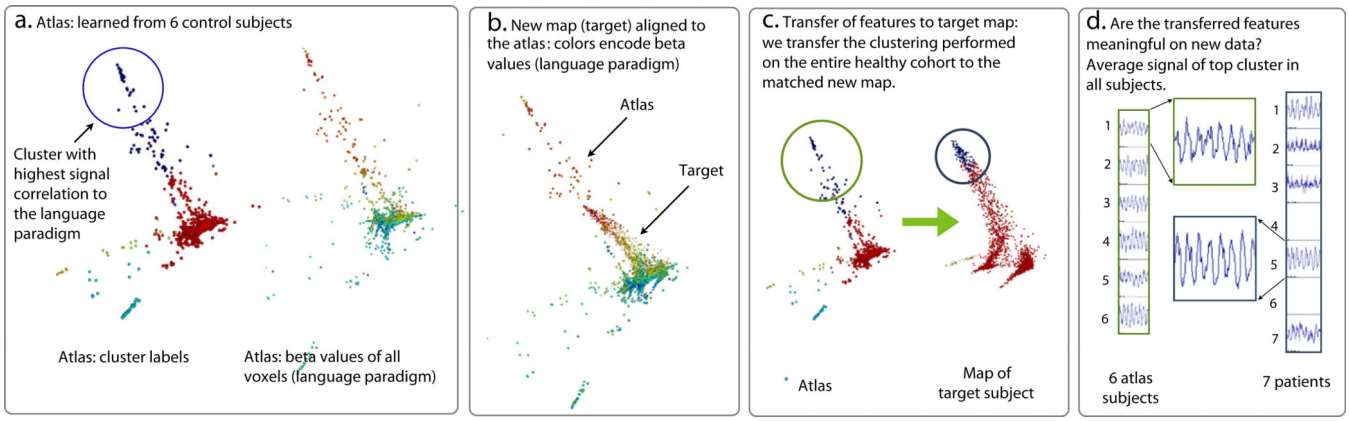

Figure 7.

Transferring structure learned from the atlas population to a target subject. (a) Each point in the atlas Γ_A carries a cluster label, or activation information; (b) An embedding map of the new data is aligned to the atlas; (c) Labels are transferred from the atlas to the new subject map; (d) the cluster that includes active areas of all atlas subjects is mapped to voxels in the patient population that show similar activation profiles.

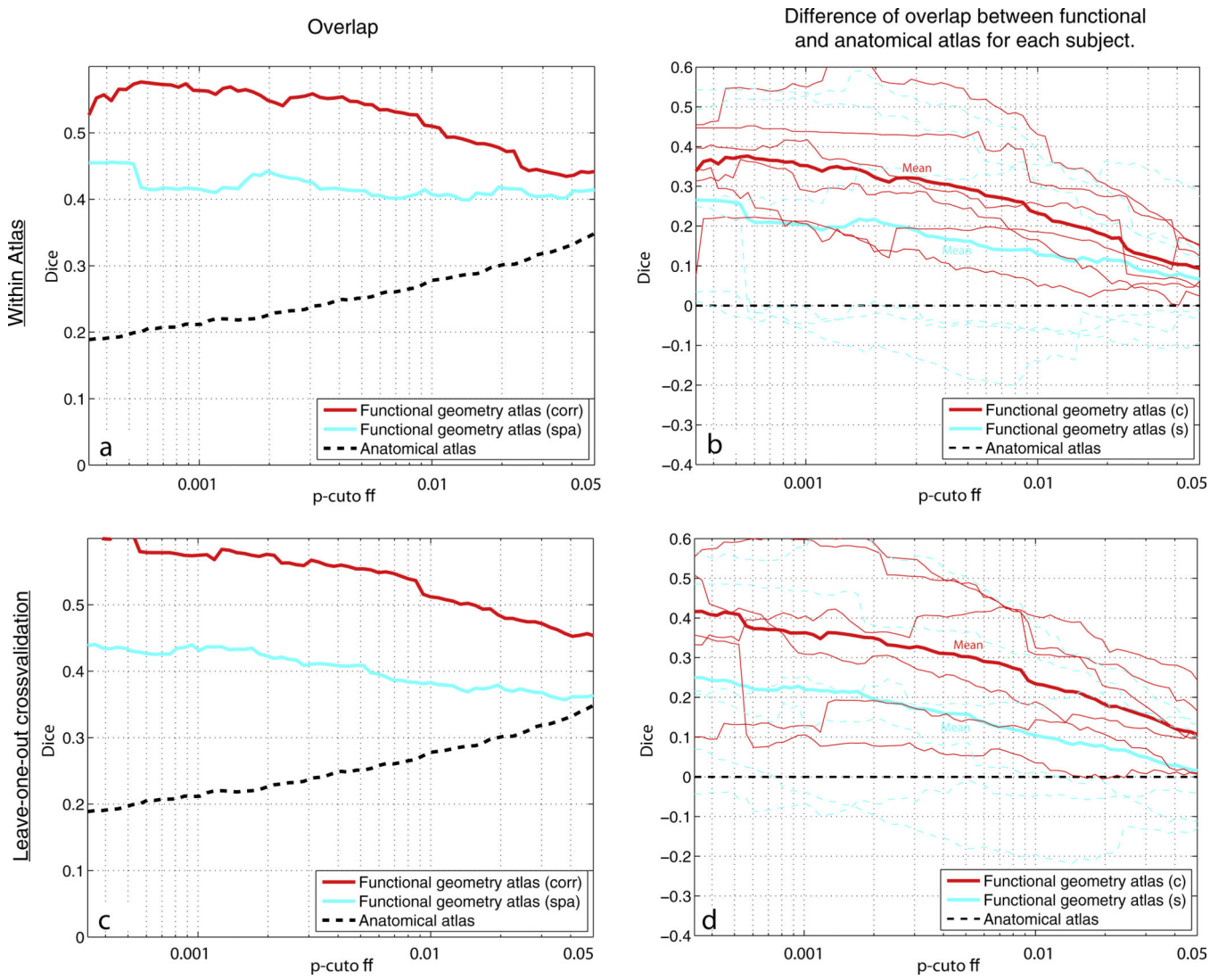

Figure 8.

Matching active areas from the atlas to individual control subjects. All plots report volume overlap between regions predicted by the atlas and active regions in the individual detected by GLM as a function of the p-value cutoff used by the detector. The p-value cutoff in the group analysis determines the number of voxels included in the matching. We then match an equal amount of the lowest p-value voxels between group-level and subject-specific maps. Mapping within the atlas: (a) Mapping overlap (average Dice scores) when predicting activated regions in a control subject from the other atlas subjects; (b) Increase in volume overlap offered by the functional atlas over the anatomical atlas. Leave-one-out-cross-validation: (c)Mapping overlap when predicting activated regions in a control subject not included in the atlas from the atlas subjects; (d) Increase in volume overlap offered by the functional atlas over the anatomical atlas. Red: initial orthonormal alignment was based on fMRI signal correlation, cyan: initial orthonormal alignment was based on the spatial position in the MNI atlas. Black dashed lines represent anatomical alignment (MNI). Thin lines in (b) and (d) correspond to individual subjects.

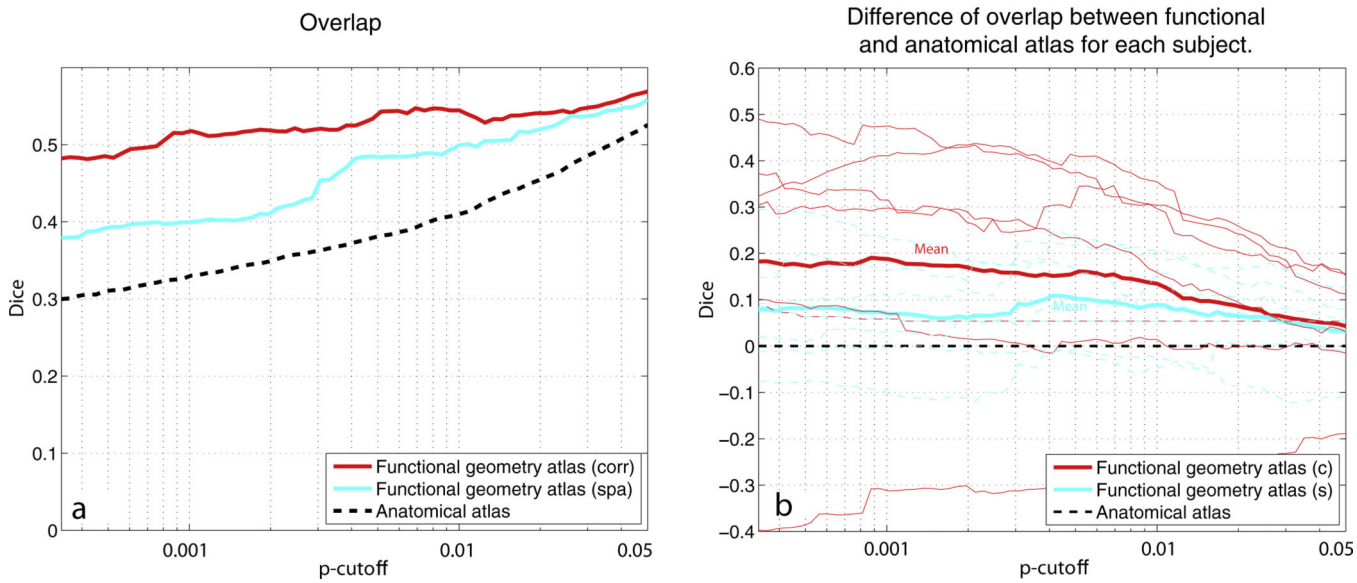

Figure 9.

Matching active areas from the atlas to tumor patients. All plots report overlap between regions predicted by the atlas and active regions detected by GLM as a function of the p-value cutoff used by the detector. The p-value cutoff in the group analysis determines the number of voxels included in the matching. We then match an equal amount of the lowest p-value voxels between group-level and subject-specific maps. (a)Mapping overlap when predicting activated regions in a patient from the atlas subjects; (b) Increase in volume overlap offered by the functional atlas over the anatomical atlas. The red/cyan lines represent functional alignment. Red: initial orthonormal alignment was based on fMRI signal correlation, cyan: initial orthonormal alignment was based on spatial position in the MNI atlas. Black dashed lines represent anatomical alignment (MNI). Thin lines in (b) correspond to individual subjects.